REPORT DOCUMENTATION PAGE

Form Approved
OMB No. 0704-0188

1. REPORT DATE *(DD-MM-YYYY)*	2. REPORT DATE	3. DATES COVERED *(From - To)*
30-09-2018	Final Report	Aug 2015 - Sep 2018

4. TITLE AND SUBTITLE

ESTIMATION OF WATER COLUMN AND SEDIMENT ACOUSTIC PROPERTIES USING A DISTRIBUTED NETWORK OF SONOBUOYS: A SIMULATION STUDY AND FIELD EXPERIMENT DATA ANALYSIS (FINAL REPORT)

5a. CONTRACT NUMBER
N00014-15-P-5114

5b. GRANT NUMBER

5c. PROGRAM ELEMENT NUMBER

6. AUTHOR(S)

RAJAN, Dr. Subramaniam D. - Scientific Solutions, Inc.

5d. PROJECT NUMBER

5e. TASK NUMBER
CLIN 0004AD

5f. WORK UNIT NUMBER

7. PERFORMING ORGANIZATION NAME(S) AND ADDRESS(ES)

Scientific Solutions Inc. - 99 Perimeter Rd., Nashua, NH 03063

8. PERFORMING ORGANIZATION REPORT NUMBER

F095-18-0930

9. SPONSORING/MONITORING AGENCY NAME(S) AND ADDRESS(ES)

Office of Naval Research
875 North Randolph Street, Suite 1425
Arlington, VA 22203-1995

10. SPONSOR/MONITOR'S ACRONYM(S)
ONR

11. SPONSORING/MONITORING AGENCY REPORT NUMBER

12. DISTRIBUTION AVAILABILITY STATEMENT

DISTRIBUTION STATEMENT A: Distribution approved for public release; distribution is unlimited.

13. SUPPLEMENTARY NOTES

14. ABSTRACT

The US Navy's Multi-Static Active Coherent (MAC) acoustic search system is an air-launched system that combines a coherent source sonobuoy with a field of receiver sonobuoys. The operational search data collected during MAC exercises are well suited for post-processing to infer water column and sediment acoustic properties. We present results of simulation studies done to determine feasibility of estimating complete set of acoustic properties of the water column and sediments over a wide area by using a distributed network of receiver sonobuoys coupled with a source sonobuoy that transmits a broadband signal. The inversions based on mode dispersion data estimated from the signals acquired by the receiver sonobuoys were carried out with data from a range of frequency bands. We show that the inversions can yield acceptable estimates of the water column and sediment properties. Analysis of data collected during a field experiment, which mimics the operational scenario of MAC, is also presented. Inversions carried out with this experimental data provide estimates of water column and sediment acoustic properties. Evaluation of the inversion results show that the estimated sediment parameters are consistent with bottom models obtained for this general experimental area by other investigators.

15. SUBJECT TERMS

Inverse problem, Shallow Water Acoustics, Modal inverse

16. SECURITY CLASSIFICATION OF:			17. LIMITATION OF ABSTRACT	18. NUMBER OF PAGES	19a. NAME OF RESPONSIBLE PERSON
a. REPORT	b. ABSTRACT	c. THIS PAGE			Dr. Subramaniam D. Rajan
U	U	U	SAR	54	19b. TELEPONE NUMBER (*Include area code)* (603) 880-3784

Scientific Solutions, Inc.
INNOVATIVE RESEARCH AND ENGINEERING

UNCLASSIFIED

DISTRIBUTION STATEMENT A:
Distribution approved for public release; distribution is unlimited.

ESTIMATION OF WATER COLUMN AND SEDIMENT ACOUSTIC PROPERTIES USING A DISTRIBUTED NETWORK OF SONOBUOYS: A SIMULATION STUDY AND FIELD EXPERIMENT DATA ANALYSIS (FINAL REPORT)

Contractor:
Scientific Solutions, Inc.
Dr. Subramaniam D. Rajan
99 Perimeter Road
Nashua, NH 03063-1325

Contract No: N00014-15-P-5114

CLIN Item 0004AD / CDRL D001

Reporting Period: 10/1/2017 – 09/30/2018

ONR Long Range Broad Agency Announcement (BAA) 15-001 for Navy and Marine Corps Science and Technology published in FedBizOpps on 29 September 2014

SSI Report Number: F095-18-0930

Date: 09/30/2018

Technical Point of Contact:
Office of Naval Research
Dr. Robert Headrick Code: 32
875 North Randolph Street
Arlington, VA 22203-1995

UNCLASSIFIED

ESTIMATION OF WATER COLUMN AND SEDIMENT ACOUSTIC PROPERTIES USING A DISTRIBUTED NETWORK OF SONOBUOYS: A SIMULATION STUDY AND FIELD EXPERIMENT DATA ANALYSIS (CLIN: 0004AD- FINAL REPORT)

Office of Naval Research
Contract No: N00014-15-P-5114
SSI Project No: F095

ABSTRACT

The US Navy's Multi-Static Active Coherent (MAC) acoustic search system is an air-launched system that combines a coherent source sonobuoy with a field of receiver sonobuoys. The operational search data collected during MAC exercises are well suited for post-processing to infer water column and sediment acoustic properties. We present results of simulation studies done to determine feasibility of estimating complete set of acoustic properties of the water column and sediments over a wide area by using a distributed network of receiver sonobuoys coupled with a source sonobuoy that transmits a broadband signal. The inversions based on mode dispersion data estimated from the signals acquired by the receiver sonobuoys were carried out with data from a range of frequency bands. We show that the inversions can yield acceptable estimates of the water column and sediment properties. Analysis of data collected during a field experiment, which mimics the operational scenario of MAC, is also presented. Inversions carried out with this experimental data provide estimates of water column and sediment acoustic properties. Evaluation of the inversion results show that the estimated sediment parameters are consistent with bottom models obtained for this general experimental area by other investigators.

ANTICIPATED BENEFITS:

The methods can be adopted to characterize the water column and the sediment using data acquired in routine operational exercises of the Navy.

KEYWORDS:

Inverse problem, Shallow water acoustics, Modal inverse

TABLE OF CONTENTS

ACKNOWLEDGEMENT

The author wishes to thank George V Frisk, Scientist Emeritus, Woods Hole Oceanographic Institution, MA, for providing the data of the field experiment (MOMAX V) analyzed in this report. This experiment was part of Navy's Rapid Transition Project.

TABLE OF FIGURES/TABLES

FIGURES

TABLES

1.0 SUMMARY

Estimation of sediment acoustic properties in shallow water areas of the ocean has been an area of research for many years. The shallow water environment is highly variable from one location to the next and there is therefore a need to estimate the sediment properties over a wide area of interest. In this context, this report studies the possibility of using data collected during routine acoustic search system such as the US Navy's Multi-Static Active Coherent (MAC) acoustic system for estimating the acoustic properties in a shallow water area. One part of this report is a simulation study, which investigates the ability of estimating the water column and sediment acoustic properties over a wide area using a distributed network of receiver sonobuoys in conjunction with a source sonobuoy in a situation similar to the MAC acoustic search system. The source sonobuoy transmits a broadband signal. These are acquired by the receiver buoys. Analysis of the acquired signal provides mode dispersion data. A linearized method for estimating the water column and sediment properties from the mode dispersion data is used to determine the water column and sediment properties over a wide area. The simulation study demonstrates that acceptable estimates of the water column and sediment acoustic properties can be obtained by this approach. In performing this analysis, the only parameter that has been assumed as known is the water column depth, which in most cases is available from archival data. In the second part of the paper, we analyze data collected in a field experiment. This field experiment mimics the acoustic search system in that the source transmitted a broadband signal from several discrete locations over a wide area. These signals were acquired by freely drifting buoys. The signal acquired by the buoys is analyzed to estimate the mode dispersion data from which the water column and sediment acoustic properties are inferred. The results of this analysis shows that the bottom models obtained are consistent with bottom models obtained by analysis of narrow band during the same experiment as well as with models predicted by other investigators who have performed experiments in the general area. The simulation study and the analysis of the experimental data clearly demonstrate the capability of estimating the water column and sediment properties over a wide area using a network of buoys.

2.0 INTRODUCTION

In shallow water, the acoustic properties of the seabed play a critical role in affecting propagation and reverberation, and therefore detection and localization. Unlike the deep-water situation, where the seabed can be characterized by a relatively small number of provinces, the shallow-water environment is highly variable from one locale to the next, thus requiring geoacoustic information for the specific areas of strategic interest.

The US Navy's Multi-Static Active Coherent (MAC) acoustic search system is an air launched acoustic search system that combines a coherent source sonobuoy with a field of receiver sonobuoys. The operational search data collected during MAC exercises are well suited for post-processing to infer acoustic properties of the water column and sediments. The acoustic properties in shallow water can be estimated using inversion methods that use modal data such as modal eigenvalues or mode travel times as input data. A number of papers have been published where the mode dispersion data are used to estimate the sediment parameters [1,2,3,4]. Different methodologies are employed for estimating the sediment parameters from experimentally determined mode dispersion data. It varies from linearized inverse procedure based on perturbation theory to full non-linear inversion based on Bayesian theory. In the analysis presented in this paper, we use the linearized inversion procedure and estimate the water column and sediment properties.

The paper is organized as follows. In Section 3.1, we provide a brief description of the inversion methodology. A description of the simulation study to investigate the estimation of the waveguide

properties over a wide area using a distributed network of sonobuoys is presented in Section 3.2. A discussion of the results of the simulation study is presented in Section 3.3. In Section 3.4, we provide a description of the broadband component of experiment MOMAX V. The mode dispersion data estimated by analysis of signals acquired by the receiver sonobuoys are used to perform the inversions and the results of the inversions are presented. Discussion of the results of the experimental data analysis is presented in Section 3.5. The project accomplishments that summarize the results of the simulation study and the analysis of experimental data are presented in the final section.

3.0 METHODS, ASSUMPTIONS, AND PROCEDURES OF TASKS PERFORMED

3.1. INVERSION PROCEDURE

Consider a range-independent ocean model whose compressional wave speed and density are represented by $c_b(z)$ and $\rho_b(z)$, respectively. For this model, k_n and ϕ_n are the eigenvalue and mode function of the *n*th mode, respectively, that satisfy the Helmholtz equation and boundary conditions associated with the waveguide model. We now perturb the compressional wave speed by a small quantity $\Delta c(z)$. This will result in a change in the group speeds of the propagating modes. It has been shown that the change in group speed of the *n*th mode due to the perturbation of the compressional wave speed is given by[5].

$$\frac{1}{\nu_n(\omega)} - \frac{1}{\hat{\nu}_n(\omega)} = \frac{\partial}{\partial\omega}\int_0^\infty \frac{1}{k_n(\omega)} \frac{\omega^2 \Delta c(z)}{c_b^3(z)\rho_b(z)} \left|\phi_n(z,\omega)\right|^2 dz. \tag{1}$$

In the above equation ν_n and $\hat{\nu}_n$ represent the group speeds of mode *n* for the unperturbed and the perturbed ocean models, respectively, and ω is the frequency of the acoustic source.

The mode travel time is obtained by dividing the range between the source and receiver by the group speed of the mode in question, such that the term on the left hand side of Eq. (1) is related to the perturbation in mode arrival time and is given by

$$dt_n = \frac{r}{\nu_n(\omega)} - \frac{r}{\hat{\nu}_n(\omega)}. \tag{2}$$

where dt_n is the perturbation in mode travel time and *r* is the range to the receiver.

By discretizing the waveguide environment in depth, the integral in Eq. (1) is approximated by a sum as given below

$$\frac{1}{\nu_n(\omega_m)} - \frac{1}{\hat{\nu}_n(\omega_m)} = \sum_{q=1}^{Q} G_{nq}(\omega_m)\Delta c(z_q). \tag{3}$$

This sum can be reduced to a matrix equation of the form $\boldsymbol{d} = \boldsymbol{G}\boldsymbol{m}$ where $\boldsymbol{d}$ is a vector containing the perturbation in modal travel times for different modes and at different frequencies, $\boldsymbol{G}$ is a matrix whose elements are $\boldsymbol{G}_{nq}$, representing the background model, and $\boldsymbol{m}$ is a vector that contains $\Delta c\ (z)$, the perturbations to the compressional wave speed profile. The matrix equation is then inverted to determine the quantity $\Delta c(z_q),\ q = 1, \Lambda\ , Q.$

A procedure to jointly estimate the compressional wave speed and density profiles from modal eigenvalues is presented in Ref. 6. This is now modified to estimate the compressionalwave speed and density profiles from mode dispersion data.This procedure is also a linearized solution which is based on perturbation theory. Consider a range-independent horizontally stratified ocean model with iso-velocity and iso-density layers. The compressional wave speed and density in the *m*th layer are represented by c_{bm} and ρ_{bm}, respectively. For this model $k_{bn} and\ \varphi_{bn}(z)$ are the eigenvalue and mode function of the *n*th mode. We now perturb the compressional wave speed and density of the mth layer by small quantit*ies* $\Delta c_m\ and\ \Delta\rho_m$. The resulting change in modal eigenvalue is given by

$$\Delta k_n = \frac{-\omega^2\Delta c_m}{c_{bm}^3\rho_{bm}k_{bn}}\int_{z_m}^{z_{m+1}} p_{bn}^2(z)dz + \frac{\Delta\rho_m}{4\rho_{bm}^2k_{bn}}\frac{d}{dz}p_{bn}^2(z)\Big|_{z_m}^{z_{m+1}} \tag{4}$$

Equation (4) can be extended to a case when changes occur in all the layers. By taking the derivate of (4) with respect to frequency, the changes in eigenvalues as presented in the left hand side of (4) can be changed to changes in mode group speed. The resulting expression is

$$\begin{aligned}\frac{1}{\gamma_n(\omega)} - \frac{1}{\hat{\gamma}_n(\omega)} = \frac{d}{d\omega}\left\{\frac{\omega^2\Delta c_m}{c_{bm}^3\rho_{bm}k_{bn}}\int_{z_1}^{z_2} p_{bn}^2(z)dz + \cdots + \frac{\omega^2\Delta c_m}{c_{bm}^3\rho_{bm}k_{bn}}\int_{z_M}^{\infty} p_{bn}^2(z)dz\right\} \\ + \frac{d}{d\omega}\left\{\frac{\Delta\rho_m}{4\rho_{bm}^2k_{bn}}\frac{d}{dz}\left[p_{bn}^2(z)\right]\Big|_{z_1}^{z_2} + \cdots + \frac{\Delta\rho_m}{4\rho_{bm}^2k_{bn}}\frac{d}{dz}\left[p_{bn}^2(z)\right]\Big|_{z_M}^{\infty}\right\} \\ m = 1,\cdots,M \quad and\ n = 1,\cdots,N\end{aligned} \tag{5}$$

In the above equation, $\boldsymbol{\gamma_n}$and $\boldsymbol{\hat{\gamma}_n}$represent the group speeds of mode *n* for the perturbed and the unperturbed ocean models, respectively. Equation (5) is then reduced to a matrix equation of the form

$$\Delta\boldsymbol{\gamma} = \{\boldsymbol{A}|\boldsymbol{B}\}\begin{bmatrix}\Delta\boldsymbol{P_1}\\ \vdots \\ \Delta\boldsymbol{P_{2M}}\end{bmatrix} \tag{6}$$

where the vector $[\Delta\boldsymbol{P_1}\cdots\Delta\boldsymbol{P_{2M}}]^{\boldsymbol{T}}$ represents the corrections to the compressional wave speed and density of the M layers.

The elements of the matrices $\boldsymbol{A}$ and $\boldsymbol{B}$ and the vector $\Delta\boldsymbol{\gamma}$ are

$$\begin{aligned}\boldsymbol{A}_{nk} &= \frac{d}{d\omega}\left\{\frac{\omega^2\Delta c_k}{c_{bk}^3\rho_{bk}k_{bn}}\int_{z_k}^{z_{k+1}} p_{bn}^2(z)dz\right\} \\ \boldsymbol{B}_{nm} &= \frac{d}{d\omega}\left\{\frac{\Delta\rho_m}{4\rho_{bm}^2k_{bn}}\frac{d}{dz}\left[p_{bn}^2(z)\right]\Big|_{z_m}^{z_{m+1}}\right\} \\ \Delta\gamma_n &= \frac{1}{\gamma_n(\omega)} - \frac{1}{\hat{\gamma}_n(\omega)}, \qquad n = 1,\cdots,N\end{aligned} \tag{7}$$

In the case of a range-dependent environment, the modal travel time perturbation for the nth mode caused by changes in the compressional wave speed is given by[1]

$$dt_n = \frac{\partial}{\partial\omega}\int_0^r\int_0^\infty \frac{1}{k_n(s,\omega)}\frac{\omega^2\Delta c(s,z)}{c_b^3(s,z)\rho_b(s,z)}\left|\phi_n(s,z,\omega)\right|^2 dsdz. \tag{8}$$

For a given source/receiver geometry, we divide the total range *R* between the source and receiver into *P* range-independent segments. The water column and sediment properties are a function of depth only in each range-independent section. By discretizing the environment in both range and depth, the double integral can be changed into a double sum as given below

$$dt_{n,\omega} = \sum_{p=1}^{P}\sum_{q=1}^{Q} G_{npq}(\omega, s_p, z_q)\Delta c(s_p, z_q). \tag{9}$$

If $v_{n,\omega}(p)$ is the group velocity of mode *n* at frequency ω in section *p* for the perturbed ocean model and $\hat{v}_{n,\omega}(p)$ is the group velocity of mode *n* at frequency ω in section *p* for the unperturbed ocean model, the travel time difference $dt_{n,\omega}$ is given by

$$dt_{n,\omega} = \sum_{p=1}^{P} \frac{r_p}{v_{n,\omega}(p)} - \sum_{p=1}^{P} \frac{r_p}{\hat{v}_{n,\omega}(p)}. \tag{10}$$

In a field experiment, the experimentally determined mode travel time will be the second term on the right hand side of Eq. (10), and the first term is the sum of the mode travel times along the different sections as it travels from source to receiver, and these will be determined by the assumed initial background model for each section.

As was done previously, considering the set of linear equations in Eq. (9) for all modes *n* and frequencies ω, this double sum can be reduced to a matrix equation that is solved to determine the quantity $\Delta c(s_p, z_q),\ p = 1,\Lambda\ ,P, q = 1,\Lambda\ ,Q,$ where s_p refers to the *p*th step in range and z_q refers to the *q*th step in depth. Similar extension to deal with range dependent scenarios can also be made when estimating jointly the water column sound speed profile, the sediment compressional wave speed profile and density profile. Equation (9) is then put in the form of a matrix equation $\boldsymbol{Gm} = \boldsymbol{d}$ and solved for *m*, which represents the corrections to the water column sound speed, the sediment compressional wave speed and the sediment density in each range interval.

In order to solve this range-dependent problem, a multiplicity of source/receiver combinations is necessary[1]. By using a multiplicity of sources and receivers, a set of signals corresponding to each source/receiver combination is generated. Time-frequency analysis of the received signals gives an estimate of the arrival times for each mode at different frequencies along the paths of each source/receiver combination. These data are the input to the inversion algorithm.

The matrix equation to be solved is generally ill-conditioned and requires some form of regularization to obtain stable, meaningful solutions. Qualitative Regularization (QR) [7, 8] is chosen to solve the discrete inverse problem. QR is an extension of Tikhonov regularization[9], an approach that places a constraint on derivatives of the solution that ensures smoothness. QR allows for piecewise smooth solutions, and can incorporate *a priori* information to represent layered media. When this constraint is included, the solution is found by satisfying both the data and the constraint. In QR, the following equations must be satisfied

$$\boldsymbol{Gm} = \boldsymbol{d}$$

$$\boldsymbol{L_q = 0} \tag{11}$$

The operator $\mathbf{L_q}$ is defined by

$$\boldsymbol{L_q = L\left(I - \sum_{i=1}^{r} q_i q_i^T\right)} \tag{12}$$

where $\boldsymbol{L}$ is a discrete version of the differential operator $\frac{d^n}{dz^n}$, as used in Tikhonov regularization and the set of vectors $\{\mathbf{q}_i\}_{i=1}^{r}$ is an orthogonal basis for the subspace *Q* that contains all models that have discontinuities at the prescribed locations. For *n* = 2 the differential operator results in a piecewise smooth solution. The least squares solution to Eq. (11) is given by

$$\boldsymbol{\hat{m} = \left(G^T G + \lambda^2 L_q^T L_q\right)^{-1} G^T d} \tag{13}$$

In the above equation, $\hat{\boldsymbol{m}}$ is the solution, λ is a Lagrange multiplier, and T represents a transpose.

When inverting for water column sound speed along with sediment properties additional constraints are necessary. These constraints prevent any changes at prescribed locations while performing inversions. To obtain stable and reliable estimates for the water column sound speed the initial assumed values for the water column sound speed close to the ocean surface and bottom are restricted to remain unchanged by the inversion process. With this additional constraint, known as approximate equality constraint[10], the solution satisfies the data and the constraints as indicated below.

$$\begin{aligned} \boldsymbol{Gm} &= \boldsymbol{d} \\ \boldsymbol{L_q} &= \boldsymbol{0} \\ \boldsymbol{Am} &= \boldsymbol{\alpha} \end{aligned} \tag{14}$$

The matrix $\boldsymbol{A}$ identifies the location where approximate equality constraint is applied and $\boldsymbol{\alpha}$ is a vector of zeros. The least squares solution in this case is

$$\boldsymbol{\hat{m} = \left(G^T G + \lambda_1 L_q^T L_q + \lambda_2 A^T A\right)^{-1} G^T d} \tag{15}$$

The quantities $\boldsymbol{\lambda_1}$ and $\boldsymbol{\lambda_2}$ are Lagrange multipliers chosen to achieve a stable solution.

In order to estimate the water column sound speed profiles, sediment compressional wave speed profiles and density profiles, we assume that we have some approximate estimates of these profiles from archival data or some other source. These estimates of the profiles are then used as the initial background models for the inversion algorithm. The true water column sound speed, sediment compressional wave speed profiles and density profiles are small perturbations to these initial estimates of the profiles. The modal group speeds estimated from data and modal group speed calculated for the background model, are the input to the inversion process that estimates the perturbations $\Delta c\,(s,z)$ and $\Delta\rho(s,z)$. The perturbation profile is added to the initial background model to obtain the true model. In practice, the inversion is carried out iteratively, with the background model updated by $\Delta c\,(s,z)$ and $\Delta\rho(s,z)$ after each inversion calculation. After several iterations, the difference between group speeds estimated from field data and the updated models approaches zero. These updated models are taken as the result of the inversion procedure.

The reliability of the inverse results is assessed by estimating the covariance of the estimated model parameters. To obtain the covariance of the model parameters we follow the procedure outlined in Ref. 11. The basic equation for obtaining a solution of model parameters is of the form $\boldsymbol{m} = \boldsymbol{G^{-1}d}$. For errors in the data, the error in solution of model parameters will be $\Delta\boldsymbol{m} = \boldsymbol{G^{-1}}\Delta\boldsymbol{d}$. Then $\boldsymbol{C_m}$ the variance of the model parameters is then given by

$$\langle(\Delta\boldsymbol{m}\Delta\boldsymbol{m^T})\rangle = \boldsymbol{G^{-1}}\langle\Delta\boldsymbol{d}\Delta\boldsymbol{d^T}\rangle\left(\boldsymbol{G^{-1}}\right)^{\boldsymbol{T}} \tag{16}$$

$$\boldsymbol{C_m} = \boldsymbol{G^{-1}C_d}\left(\boldsymbol{G^{-1}}\right)^{\boldsymbol{T}} \tag{17}$$

The data covariance matrix $\boldsymbol{C_d}$ is estimated from the data using the procedure outlined below.

1. In cases where only a single received signal is available for analysis, as in the simulation study, we assume that the data covariance matrix is represented by $\boldsymbol{C_d} = \gamma_k\boldsymbol{I}$ where **I** is an identity matrix and γ_k is the variance of the data corresponding to the kth mode. We now assume that the variance of the data is the variance between the observed data and the data predicted by the model obtained at final stage of the inversion. This is the result in Ref. 4 for the maximum variance of the data. The variance of mode travel time in respect of the kth mode is given by $\gamma_k = |\boldsymbol{d}_k - \boldsymbol{d}(\boldsymbol{m})_k|^2/N$. In this expression $\boldsymbol{d}_k$ is the data vector that represents the mode travel of the kth mode, $\boldsymbol{d(m)}_k$ is the vector that has the mode travel time of the kth mode for the inverted bottom model represented by $\boldsymbol{m}$ and N is the number of elements in the vectors $\boldsymbol{d}_k$ and $\boldsymbol{d}(\mathbf{m})_k$.

2. In the cases where there are multiple signals acquired by the receiver sonobuoys from source at the same location, analysis of the multiple signals provides information for estimating the data covariance matrix.

Another factor in the evaluation of the results of the inversion is the resolution. The estimate of the model parameters is given by $\boldsymbol{m_{est}} = \boldsymbol{G^{-1}d}$. Replacing the data vector by $\boldsymbol{Gm}$, we have $\boldsymbol{m_{est}} = \boldsymbol{G^{-1}Gm}$. If $\boldsymbol{R} = \boldsymbol{G^{-1}G}$ is an identity matrix then the estimate of the model parameters is the true value. If otherwise, the estimate of the model parameters is an averaged value. The averaging is based on the row vectors of the matrix $\boldsymbol{R}$. Other expression used for obtaining the averaging matrix is $\boldsymbol{R} = \boldsymbol{G^T}\left(\boldsymbol{GG^T}\right)^{\boldsymbol{-1}}\boldsymbol{G}$. To quantify the resolution we compute the resolution length. One approach to obtain the resolution length is to use the expression $rl(n) = \frac{\sum_1^M R(n,m)^2 dz}{R(n,n)^2}$.

3.2. SIMULATION STUDY

The experimental set up to extract sediment acoustic properties consists of source sonobuoy that transmits broadband signals and several sonobuoy receiver systems. The acoustic field at a receiver placed at a distance from the source is then collected and processed to determine the group speeds of the modes at a set of discrete frequencies. This forms the data set used to obtain the acoustic properties of the waveguide. A linearized approach for estimating the sediment acoustic properties from dispersion relationship, i.e. the variation of the group speed of each mode as a function of frequency, has been detailed in the previous section.

We now present a description of a simulation study in which we have a network of sonobuoys distributed over a wide area. A source carrying sonobuoy is located in the midst of the distributed network of sonobuoy receivers. The sonobuoys in the different regions have different water column depths and different bottom properties. We explore the ability of the inverse algorithm to extract sediment properties in the different areas.

A. Simulation of Environment

The estimation of sediment properties in shallow water areas is difficult because of the bathymetry in these areas are complex giving rise to varying water column depths as well as varying sediment characteristics. In order to represent such an environment in the simulation, an area of the coast of New Jersey for which the bathymetry is well known was used in this simulation. Figure 1 shows the region that was used in creating the data for this simulation together with the locations of 25 sonobuoys and the source. The locations of the sonobuoys were obtained assuming that they were uniformly distributed over the defined limits of the region as indicated by their Longitudes and Latitudes. The area covered by the sonobuoys was then divided into six regions as shown in the right panel of Figure 1.

Using the location of the source and the buoys, the variation of the bathymetry along the lines joining the source to the source was computed and from this computation, the average depths along range intervals were determined. Because of the differences in the water column depths along the different source/buoy transects we assumed that the sediment properties also varied along these different sections. In regions where there was a large variation in water column depths, we assumed the bottom properties were different. For example in the area where Buoys 2, 19, and 20 are located there are three distinct depth regions namely region of depth 72 m followed by a region of depth 69 m and then the final section with depth of 60 m. In this case, we assumed that the regions where the depths are 72 m and 69 m have identical bottom properties whereas the region where the depth changed to 60 m has a different set of bottom properties. Similarly, by looking at the depth variations in the different parts we created seven areas with slightly different sediment properties. The left panel of Fig. 2 shows the water column depths in the different parts of the six regions. In each of these sections, we assumed different bottom models and these are termed model M1 to M7 as shown in the figure. The numbers of sediment layers and their thicknesses have also been varied and these are similar to bottom models obtained in earlier field experiments conducted in the general area used for the simulation study. In all cases, the terminating half space is assumed to have a compressional wave speed of 1850 m/s. The sediment density values were set at 1.6 gm/cc in all the layers and in the terminating half space. Attenuation in the sediment layers and terminating half space are neglected. A sound speed profile of the water column is assumed and this is plotted in the right panel of Fig. 2. This profile exists over the entire simulated area.

In the analysis presented in subsequent section, we restrict the analysis to the cases dealing with bottom models M1, M2, M3, M4 and M5. These represent a range dependent case with three sediment layers, a range-dependent case with two sediment layers and one range independent case with two sediment layers. The water column depths and the ranges that are involved in the analysis are shown in Table 1.

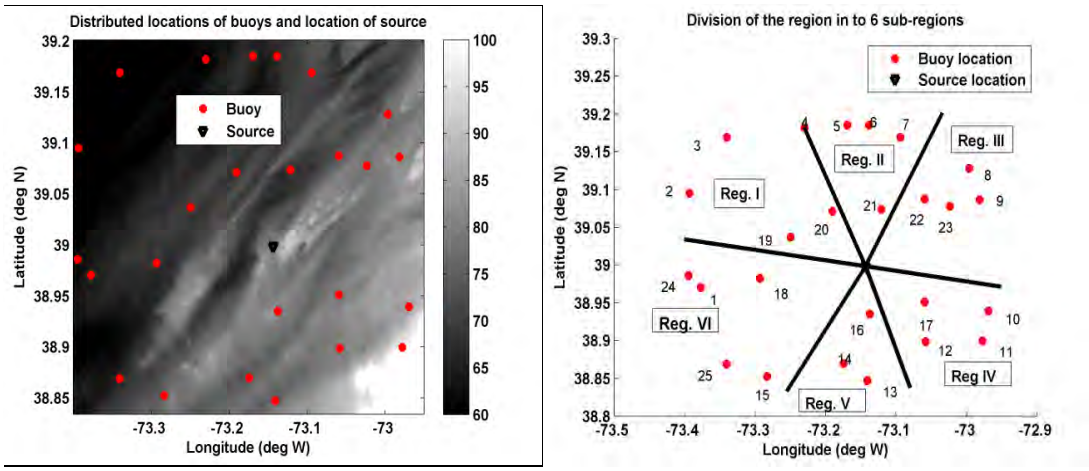

Figure 1: The left panel shows the region used in the simulation study together with the location of the distributed network of sonobuoys and the location of the source. The right panel indicates the division of the region into six areas. Each of these areas is characterized by different water column depths and sediment properties.

B. Broad band signal generation

Broadband signals that have found wide acceptance are the LFM (Linear Frequency Modulated) signal or chirp in which the frequency is varied linearly either going up or down with the signal duration. Broadband signals are also created by pseudo-random sequences[12]. The maximal length, binary, shift-register sequences are pseudorandom sequences. The sequence of zeros and ones generated by the sequence is used to modulate a carrier signal. For creating the transmitted signal the zeros in the sequence is changed to -1, (i.e. we now have a sequence of 1 and -1). Each digit in the sequence is a chip. If the sequence has N digits, the signal has N chips. The length of each chip defines the bandwidth of the signal. Based on the bandwidth requirement the number of cycles of the transmitted signal that form a chip is determined.

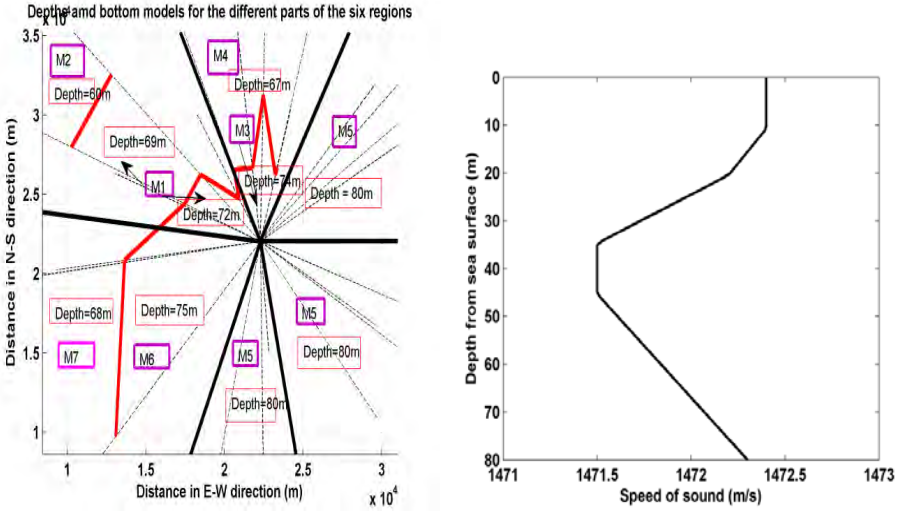

Figure 2: The water column depths in the different parts of the six regions and the corresponding bottom models are shown in the left panel. The red line demarcates regions of different depths. The right panel shows the water column sound speed profile for the simulated area.

C. Computation of Signals Acquired by the Sonobuoys

In order to compute the signal acquired by the buoys, the distances from the source to the receiver is required. These were obtained from the known positions of the source and the respective receiver buoys. A time-domain acoustic signal at the receiver can be modeled by Fourier synthesis of the frequency domain solution to the acoustic wave equation using the expression

$$p(r,z;t) = \int_{-\infty}^{\infty} S(\omega) p(r,z;\omega) \exp(i\omega t)\, d\omega \tag{18}$$

where $S(\omega)$ is the spectrum of the transmitted signal and $p(r,z;\omega)$ is the frequency domain solution at range r and depth z. To compute the time domain solution above requires that $p(r,z;\omega)$ be calculated at a number of discrete frequencies, which span the frequency band of the source spectrum. The ocean environment was the input to the normal mode code KRAKEN[13] for computing the frequency domain solution with the range to the receiver, depths of the source, and receiver set as required. The source and receiver depths were selected to make sure that all the mode functions of the modes used in the inversion have mode amplitudes such that the time frequency response of the received signal will have the modes well defined.

The signal acquired by the receiver is a convolution of the impulse response of the channel with the transmitted pulse. Before processing the signal acquired by the buoys for time-frequency analysis, it is necessary to extract the impulse response of the channel, to take out the time-frequency variation of the transmitted signal during signal duration. This is done by de-convolution of the received signal. This can be done either in the frequency domain or in time domain by cross-correlation. In the simulation study presented here, the deconvolution of the signal was done in the frequency domain.

Table 1: Variation of average depth with range from source along each source/buoy pair

Buoy No.	Range Int. (m)	Depth (m)	Range (m)	Depth (m)	Range (m)	Depth (m)
2	0-5365	72	5366-13090	69	13091-24201	60
4	0-4826	74	4827-21725	67		
6	0-9221	74	9222-20745	67		
8	0-19270	80				
19	0-5814	72	5815-10184	69		
20	0-3023	72	3024-9075	69		
21	0-4757	74	4758-8565	67		

D. Extraction of Mode Dispersion Data

The group speeds as a function of mode number and frequency can be obtained from a knowledge of the mode eigenvalues and mode functions using[14]

$$v_n(\omega) = \frac{k_n(\omega)\int_0^\infty \frac{1}{\rho(z)} |\phi_n(z,\omega)|^2 \, dz}{\omega\int_0^\infty \frac{1}{\rho(z)c^2(z)} |\phi_n(z,\omega)|^2 \, dz}. \tag{19}$$

This assumes that the environment is fully known. In a field experiment the group speed as a function of frequency and mode is obtained by performing short time Fourier transform (STFT) of the received signal. Such a transform provides the time taken by the modes to travel from source to receiver from which the mode group speeds are obtained. If the distance between the source and receiver is large, the modes are fully resolved and it is not problematic to estimate the mode dispersion curves. When the range to receiver is short the modes are not well resolved and the signals are analyzed using the warping method[15] to estimate mode travel times. The warping method involves applying a warping function to the received signal. If *g* is a function of *x*, and the warping operator is *h(x)*, the warped function $W_g(x)$ is

$$W_g(x) = \sqrt{\frac{dh}{dx}}\, g(h(x)) \tag{20}$$

The warping function applied to the received signal *s(t)* in our analysis is

$$h(t) = \sqrt{t^2 + (\tfrac{r}{c})^2} \tag{21}$$

where *r* is the distance between source and receiver and *c* in the sound speed in the water column. It has been shown that the accuracy of the quantity *r/c* is not critical and even an approximate value is adequate[16]. Any warped function can be unwarped by applying the operator $h^{-1}(t) = \sqrt{t^2 - \left(\frac{r}{c}\right)^2}$.

The estimation of the group speeds by processing the received signal *s(t)* using the warping method is accomplished in the following stages:

1. Using the warping operator determine the warped signal $s_{warped}(t)$.
2. Perform STFT of the warped signal and obtain $S_{warped}(t, f)$.
3. In this time frequency representation the modes are resolved and well separated. Each mode can now be filtered.
4. Perform inverse STFT on the warped mode and obtain the warped mode $md_{warped}(t)$.
5. Unwarp the mode function to get $md(t)$ from $md_{warped}(t)$.
6. Perform STFT of $md(t)$ to obtain the mode dispersion curve for the modes.

In Figure 3, different steps of the warping procedure are shown. The top left panel in the figure is the received signal. The impulse response obtained from the signal is shown in the top right panel. The impulse response obtained by performing the de-convolusion of the received signal. The bottom left panel shows the signal to which the warping operator has been applied. The bottom right panel shows the time-frequency representation of the warped signal. The modes are well resolved in this representation and each mode can be filtered by simply masking modes those that are not of interest. After filtering out each mode these are

unwarped and the STFT is performed on the unwarped signal to get mode dispersion curve for the extracted mode.

3.3. ANALYSIS OF DATA AND DISCUSSION OF RESULTS

The mode dispersion data estimated from the signals acquired by the various sonobuoys distributed over the area is now used to extract the acoustic characteristics of the water column and the sediments. This involves estimating the following parameters.

1. The speed of sound in the water column.
2. The compressional wave speed and density of the sediment layers and the terminating half space.
3. The total thickness of the sediment and the layering information.

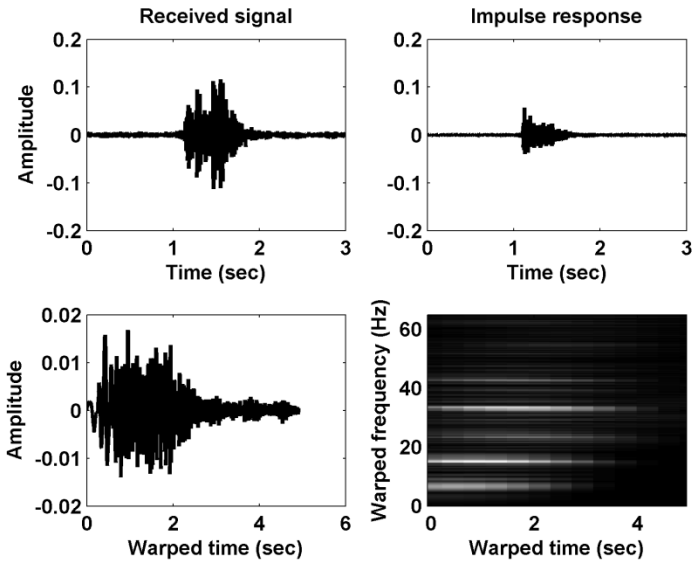

Figure 3: Four stages in the processing of the signal using warping operation are presented. Top left panel shows the received signal, the top right signal shows the impulse response after performing the deconvolution of the signal. The bottom left panel shows the signal after processing through the time warping transformation. The bottom right panel shows the time frequency response of the warped signal.

The quantities under Items 1 and 2 above is determined using the inverse procedure outlined in the earlier section. To carry out inversions the information on the layering of the sediment is required. The following procedure was adopted for estimating the number of layers and layer thicknesses. First we assume that the ocean bottom is represented by a single sediment layer followed by a terminating half space. Assuming different values for the thickness of the sediment layer, we performed inversion for the compressional wave speed of the sediment and the half space. For other parameters such as the water column sound speed profile and density of the sediment layers an average value is assumed. For each of this assumed layer thickness inversions resulted in a bottom model. The mean squared error between the mode dispersion data as predicted by the inverted model and the mode dispersion data used for the inversion was computed. The layer thickness that yields the minimum mean squared error is assumed to be the layer thickness of the sediment layers. We then proceed to determine if the sediment constitutes more than one layer. To estimate the number of layers we examine the sediment model obtained during the inversions for estimating the sediment layer thickness.

Figure 4 shows the variation of the compressional wave speed in the sediment layers while determining the total layer thickness. The left panel in the figure shows the result in the case of bottom model with two layers and a terminating halfspace. It can be easily assessed from this result that the bottom model is made up of two layers. The right panel shows similar result in a case where the bottom model has three layers. In this case also it is easy to assess that the sediment has three layers with the top and bottom layers have wave speeds much lesser than the middle layer. In the case of a two layer model, different values of thickness for each layer are assumed but with the total thickness equal to the total layer thickness determined earlier. For each combination of layer thicknesses we perform inversion and as before and determine the mean squared error between the mode dispersion values determined for the inverted model and the values used as input to the inversion process. The layer thickness values that has the least mean squared error is taken as the layer thicknesses of the layers. In cases where it is not possible to determine the layer thicknesses a one layer model is assumed to be more appropriate. Similar approach is used while determining the layer thicknesses in respect of a three layer model.

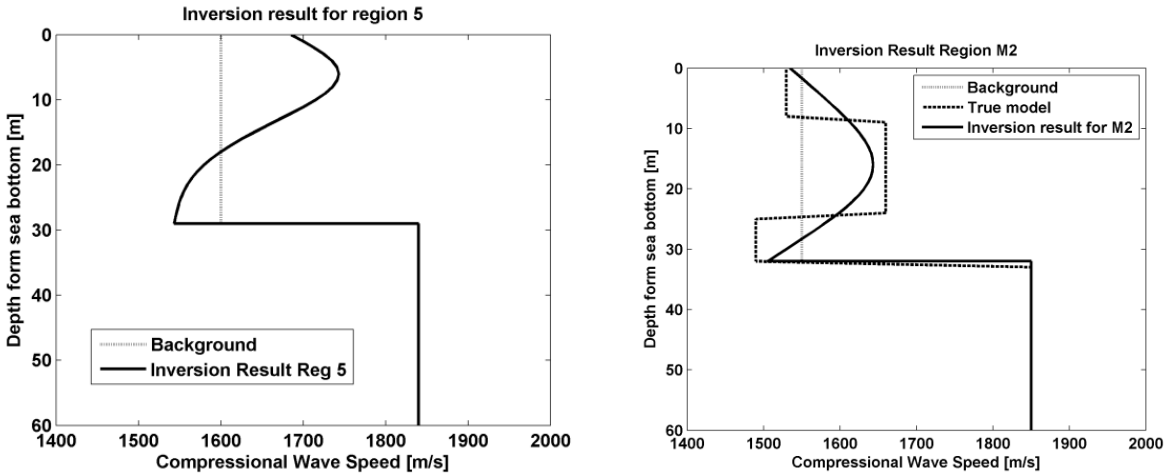

Figure 4: The left panel shows the bottom model obtained during estimation of the layer thickness in Region 5. The right panel shows result in respect of Region 2. The left panel suggests that the bottom has two layers. The result shown in the right panel suggests the presence of three layers.

In analysing data acquired in the frequency interval 250 Hz -500 Hz and other higher frequency a problem was encountered. During inversion process, a bottom model is assumed and mode travel time is calculated using Eq. (19) for this assumed model and compared with the travel time as in the data. At some of the frequencies some modes are in resonance. In the case of these modes, the amplitude of the mode function in the water column is near zero and has large values in the sediment layers. The computed mode travel time is widly different from its value at the previous mode. Also since this mode has near zero amplitude in the water column it is not excited and hence not observed in the acquired signal. Hence in the analysis of the received signal, either by STFT or warping method, this mode is not observed. Because of this it is difficult to make meaning full comparison between mode travel time from data and that from the bottom model. A detailed description of the problem and the procedure used to over come the problem is provided in Appendix.

A. Analysis of Range Independent Case

The bottom model of Region III (cf. Figure 1) is range independent. The depth of the water column is 80 m. The bottom model for this region consists of two layers with layer thicknesses of 18 m and 12 m. This is terminated by a half space. The compressional wave speed in the layers and half space are 1700 m/s, 1550m/s and 1850m/s respectively. The density is 1.6 gm/ccin the layers and half space.

Table 2: Layer thickness estimated from data

Freq. Range (Hz)	Total Thickness (m)	No. of Layers	Layer 1 (m)	Layer 2 (m)
50 - 110	30	2	17	13
250 - 310	30	2	16	14
900 - 960	22	1	22	

Analysis of simulated data were carried out in three frequency brackets namely 50 Hz – 110 Hz, 250 Hz – 310 Hz and 900 Hz – 960 Hz. The estimation of total layer thickness and the layering was done as described earlier. The results are shown in Table 2. The inversions were carried with these estimated values of layer depths. The modes that were used in the inversions are indicated in Table 3.

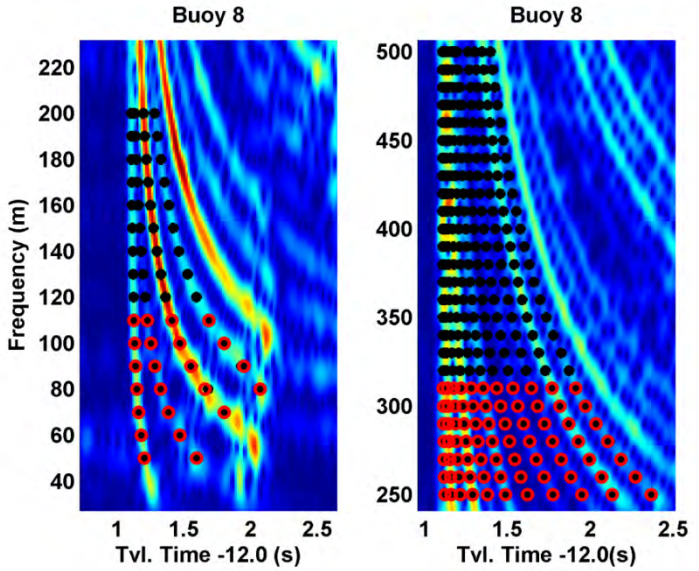

Figure 5: The travel time of modes used in the inversions as estimated from data (dots) and predicted by inverted bottom model (red circle).

Table 3: Modes used in the inversion water column sound speed and the sediment compressional wave speed and density

Frequency Range	Mode numbers	Comment
50 Hz – 110 Hz	1 to 4	50 Hz – Modes 1 - 2 60 Hz – Modes 1 - 2 70 Hz - Modes 1 - 3 80 Hz - Modes 1 - 4 90 Hz - Modes 1 - 4

Frequency Range	Mode numbers	Comment
		100 Hz - Modes 1 - 4 110 Hz - Modes 1 - 4
250 Hz – 310 Hz	2 to 12	Mode numbers same at all frequencies in 10 Hz step
900 Hz – 960 Hz	7, 9 to 21, 24 to 28, 31, 32, 34, 36, 38 to 40	Mode numbers same at all frequencies in 10 Hz step

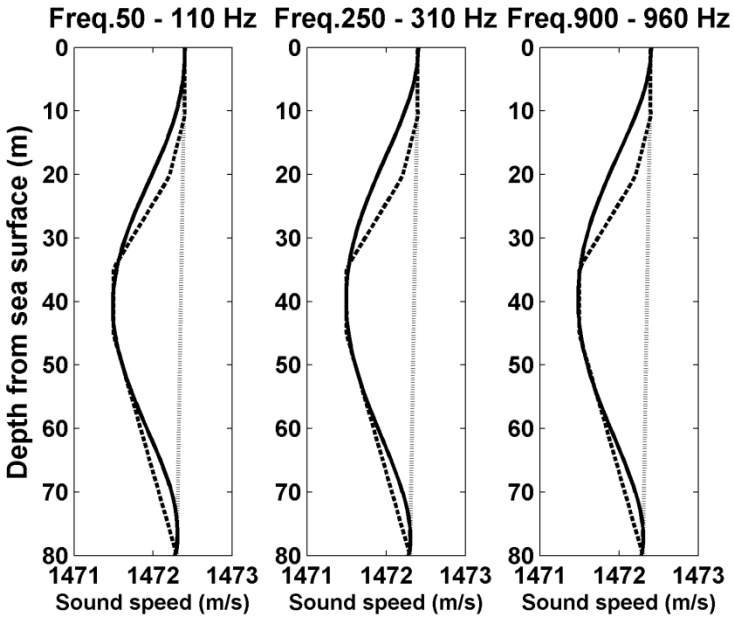

Figure 6: True sound speed profile (Full black), Initial profile (Dotted black) and inverted profile (Dashed black) at the three frequency ranges.

The agreement between the mode arrival time as estimated from data and the arrival time as predicted by the inversion results are shown in the left panel of Figure 5 for the frequency interval 50 Hz -110 Hz. Similar comparisons are made in the right panel of Figure 5 for inversions in the frequency band 250 Hz-310 Hz. The figure indicates good agreement between mode arrival time as estimated from data and the arrival time predicted by the inverted model. The water column sound speed profiles obtained by inversion (Figure 6) are quite close to the true model in all the three frequency bands even though the initial background model had a large difference with the true model. In respect of the compressional wave speed and density the inverted model values and the true values are indicated in Table 4. The agreement between the true values and the inverted results are in good agreement in respect of results obtained in the frequency interval 50 Hz – 110 Hz. In the frequency range 250 H-310 Hz there is a disagreement between the true value and the inverted result. Analysis of the mode function for the inverted bottom model shows that in the case of Modes 2 to10 the mode function has near zero values at depths greater than 15 m in the sediment layers. The other modes (Modes 11 and 12) have a small values beyond 15 m depth and therefore have limited influence over the inversion results at depths greater than 15 m. Further the use of layer thickness estimate of 16 m and 14 m for the two layers is another reason for the differences in the compressional wave speed estimates for the layers. In the case of inversions with data in the frequency range 900 Hz – 960 Hz a single layer model was assumed. In this case mode function has very low values beyond a depth

of a 5 m in to the sediment. Inversion results for this shallow depth is shown as the value over the entire sediment thickness because of the assumptions in the inversion algorithm. The deviations of the water column sound speed, deviation of the compressional wave speed and the density of the sediment layers were estimated using the procedure outlined in Section 3.1. The are shown in Tables 4A and 4B. The table also includes the resolution lengths for the inversion estimates.

Table 4: Inversion results with layer thicknesses estimated from data

Freq. (Hz)	Lay. No.	True values			Starting values		Layer thicknesses from data. Results of inversion		
		Layer Thick (m)	Com. wave Spd (m/s)	Density Gm/cc	Com. wave Spd (m/s)	Density (gm/cc)	Layer Thick (m)	Comp. wave Spd (m/s)	Density Gm/cc
50 to 110	Lay. 1	18	1700	1.6	1600	1.7	17	1704	1.571
	Lay.2	12	1550	1.6	1600	1.7	13	1564	1.571
	Half Sp.		1850	1.6	1880	1.7		1826	1.654
250 to 310	Lay. 1	18	1700	1.6	1600	1.7	16	1669	1.572
	Lay. 2	12	1550	1.6	1600	1.7	14	1577	1.572
	Half Sp.		1850	1.6	1900	1.7		1849	1.612
900 to 960	Lay.1	18	1700	1.6	1600	1.7	22	1703	1.592
	Lay2	12	1550	1.6					
	Half Sp.		1850	1.6	1900	1.7		1900	1.700

Table 4A: Deviation (Dev) and resolution lengths (RL) for the inverted model in the range independent case

Freq. range	Layer	Wave speed (m/s)		Density (gm/cc)	
		Dev (m/s)	Res. Length (m)	Dev (gm/cc)	Res. Length (m)
50 Hz to 110 Hz	Water col	0.0262	3.58		
	Layer 1	11.7	1.15	0.001	1.72
	Layer 2	7.4	2.48	0.001	1.72
	Half space	13.3	4.92	0.00037	8.10

Table 4B: Deviation (Dev) and resolution lengths (RL) for the inverted model in the range independent case

Freq. range	Layer	Wave speed (m/s)		Density (gm/cc)	
		Dev (m/s)	Res. Length (m)	Dev (gm/cc)	Res.Length (m)
250 Hz to 310 Hz	Water col.	0.025	2.07		
	Layer 1	5.85	1.94	0.08	3.23
	Layer 2	0.77	4.10	0.08	3.23
	Half space	1.28	7.00	0.28	5.55

B. Range-Dependent Case - Two Layer Bottom Model

Regions II (cf Figure 1) has two areas with varying depths namely areas where the depth of the water column is 74 m (bottom model M3) and an area where the water column depth is 67 m (bottom model M4). The sediment in both regions consists of two layer. The layers in both regions are of the same thickness but have different properties in terms of the compressional wave speed. In the case of bottom model M3 the compressional wave speed for the layers are 1700 m/s and 1550m/s. The compressional wave speed in the half space is 1850 m/s. The density is 1.6 gm/cc in the sediment layers and the half space. In respect of bottom model M4 the compressional wave speed of the layers are 1680m/sand 1500 m/s. In the terminating half space the compressional wave speed is 1850 m/s. The density is 1.6 gm/cc in the sediment layers and in the half space. To perform inversion in this range dependent environment we estimated the mode travel times from signals acquired along three different source/receiver paths. The paths used were fom the source to Buoys 4, 6, and 21. The path lengths in the two regions along these three source receiver paths are shown in Table 1.

Table 5 shows that the sediment thicknesses as estimated from the data are 30 m, 31 m, and 18 m for the three frequency bands (50 Hz -110 Hz, 250 Hz- 310 Hz, and 900 Hz – 960 Hz) used in the inversion. The two layer model for the case of inversions in the frequency band 50 Hz – 110 Hz was estimated to have thicknesses of 17 m and 13 m. In the frequency range of 250 Hz – 310 Hz the layer thicknesses are 19 m and 12 m. In the the frequency band 900 Hz -960 Hz the single layer model has a thickness of 18 m.

Table 5. Layer thickness estimated from data

Freq. range (Hz)	Total Thickness (m)	No. of Layers	Layer 1 (m)	Layer 2 (m)
50 – 110	30	2	17	13
250 – 310	31	2	19	12
900 – 960	18	1	18	

Table 6. Details of modes used in inversion

Frequency range	Mode numbers	Comment
50 Hz – 110 Hz	Modes 1 to 4 along the three source/receiver paths	50 Hz – Modes 1 - 2 60 Hz – Modes 1 - 2 70 Hz - Modes 1 – 3 80 Hz - Modes 1 - 3, 90 Hz - Modes 1 - 3, 100 Hz - Modes 1 - 3, 110 Hz - Modes 1 - 4
250 Hz – 310 Hz	1 to 10	Mode numbers same at all frequencies in 10 Hz step
900 Hz – 960 Hz	Buoy 4: 24 modes Buoy 6: 23 modes Buoy 21: 21modes	Buoy 4: 23 modes 900 Hz to 930 Hz, 24 modes 940 Hz to 960 Hz. Buoy 6: 23 modes 900 Hz to 960 Hz in 10 Hz step. Buoy 21: 21 modes 900 Hz to 960 Hz in 10 Hz step.

The comparison between the mode travel time estimated from data and that is predicted by the inverted bottom model are shown in Figures 7 and 8. The agreement between travel time estimates from data and prediction based on inverted model is excellent in the frequency band 50 Hz -110 Hz (Figure 7). However, in the case of similar comparisons at the higher frequency band (250 Hz – 310 Hz in Figure 8) a large error is seen.

This error is mainly because of error in the estimates of travel time from data. If we compare the calculated mode travel time based on the true bottom model and compare it with the travel time predicted by the inverted model an excellent agreement between the two is seen. Figure 9 shows this agreement in respect of transmissions from the source to Buoy 21. In the figure the red circle are the values as predicted by the bottom model. The black star within the red circle is the calculated travel time from the true bottom model. Similar agreements are seen in transmissions to Buoys 4 and 6.

The inversions for the water column sound speed for the two areas (i.e. Region II with water depths of 74 m and 69 m) are indicated in Figure 10. The agreement between the true sound speed profiles and the inverted model is good and all the inverted models display similar trends.

In inversions performed in the frequency bracket 50 Hz – 110 Hz, the inverted model is consistent with the true bottom model. In the inversions performed in the higher frequency ranges, inverted bottom model has acceptable values in the top layer. In the deeper layers, the inverted values are not consistent. This is mainly because the mode functions at the higher frequencies have very small values in deeper depths and does not influence the inversion results.

The deviations of the water column sound speed, deviation of the compressional wave speed and the density of the sediment layers were estimated using the procedure outlined in Section 3.1. The are shown in Tables 7A, 7B, 8A, and 8B. The tables also includes the resolution lengths for the inversion estimates.

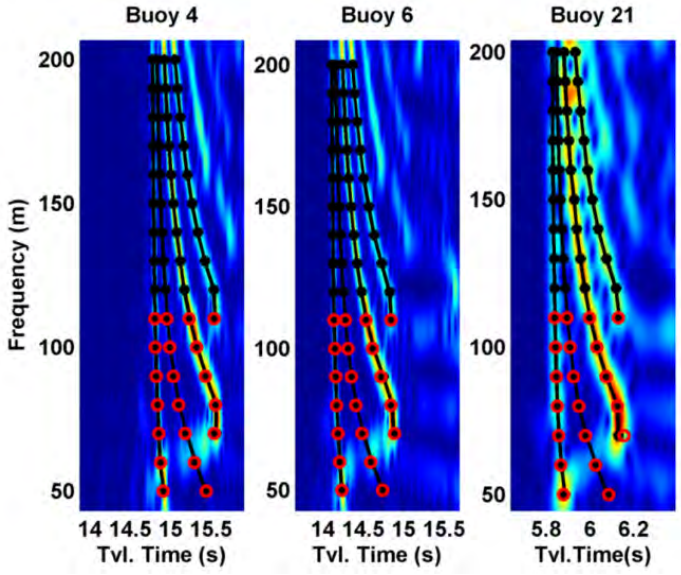

Figure 7: Travel time plots for Modes 1 to 4 from received signal in the frequency range 50 Hz – 200 Hz. These are overlaid on the spectrogram. Also shown in red circle are the travel time predictions based on the inverted model.

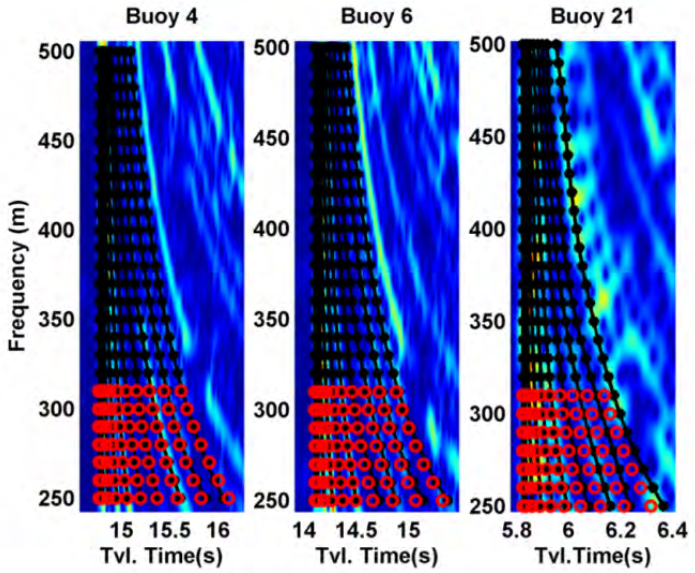

Figure 8: The three plots show the mode dispersion data for Modes 1 to 10 used in the frequency range 250 Hz – 500 Hz. The mode travel times predicted by the inverted bottom model are shown as red circles in the figure.

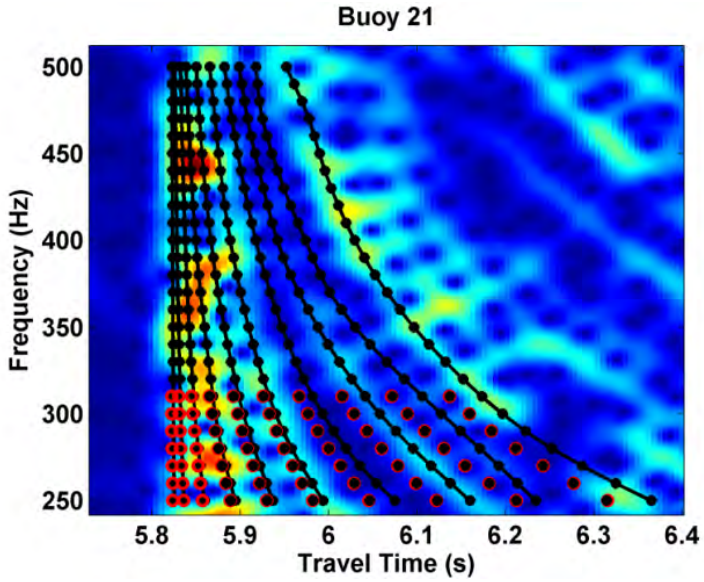

Figure 9: The mode travel time as estimated from data is overlaid on the spectrogram. The mode travel times predicted by the bottom model are the red circles. A wide difference between the two is seen. However, the travel time predicted by the bottom model is in agreement with the calculated travel time for the true bottom model for the path between the source and the Buoy 21. These are indicated as a black star within the red circle.

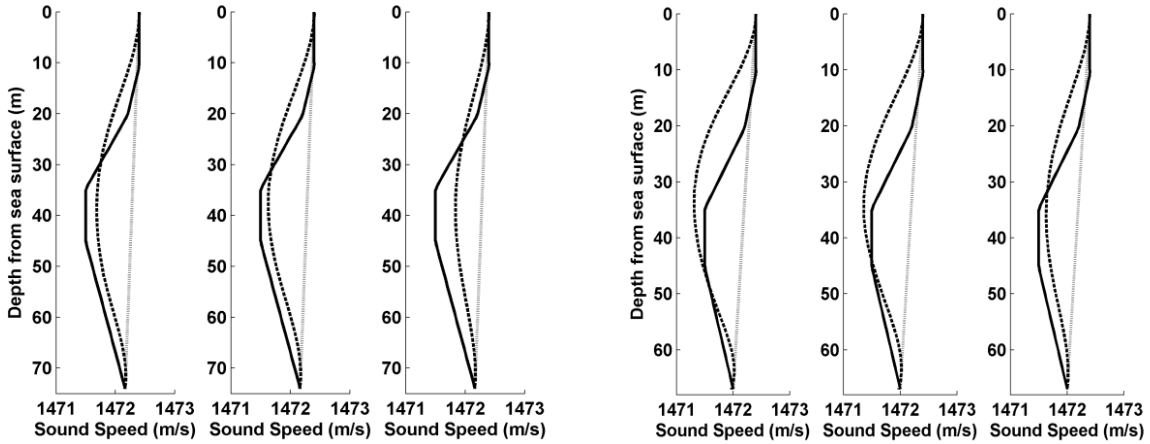

Figure 10: The left panel shows the inversion results for the water column sound speed profiles for area with water depth of 74 m. The right panel shows the result for area with water depth of 69m.. In these figures the black line represents the true profile, the dotted black line the starting profile and the dashed black line the inversion result. The three profiles in each panel are the inversion results in the three frequency ranges (i.e. 50 Hz – 110 Hz, 250 Hz – 310 Hz and 900 Hz – 960 Hz).

Table 7: Inversion results for bottom model M3 using layer thickness as estimated from data

Freq. (Hz)	Layer No.	True values			Starting values		Layer thicknesses from data Results of inversion		
		Layer Thick (m)	Comp. wave Spd (m/s)	Density Gm/cc	Comp. wave Spd (m/s)	Density (gm/cc)	Layer Thick (m)	Comp. wave Spd (m/s)	Density Gm/cc
50 to 110	Layer 1	18	1700	1.6	1600	1.7	17	1695	1.619
	Layer 2	12	1550	1.6	1600	1.7	13	1561	1.619
	Half Sp.		1850	1.6	1880	1.7		1880	1.573
250 to 310	Layer 1	18	1700	1.6	1600	1.7	19	1700	1.587
	Layer 2	12	1550	1.6	1600	1.7	12	1602	1.587
	Half Sp.		1850	1.6	1900	1.7		1900	1.700
900 to 960	Layer 1	18	1700	1.6	1600	1.7	18	1697	1.612
	Layer 2	12	1550	1.6					
	Half Sp.		1850	1.6	1900	1.7		1900	1.700

Table 7A: Deviation (Dev) and resolution lengths (RL) for the inverted model in the range dependent case (Two layer model)

Freq.range	Layer	Wave speed (m/s)		Density (gm/cc)	
		Dev (m/s)	Res. Length (m)	Dev (gm/cc)	Res.Length (m)
50 Hz to 110 Hz	Water col	0.0204	1.29		
	Layer 1	15.64	1.90	0.0024	1.80
	Layer 2	6.93	4.62	0.0024	1.80
	Half space	2.19	9.10	0.0012	8.00

Table 7B: Deviation (Dev) and resolution lengths (RL) for the inverted model in the range-independent case (Two layer model)

Freq.range	Layer	Wave speed (m/s)		Density (gm/cc)	
		Dev (m/s)	Res. Length (m)	Dev (gm/cc)	Res. Length (m)
250 Hz to 310 Hz	Water col	0.0384	2.45		
	Layer 1	10.65	1.00	0.014	1.00
	Layer 2		2.65	0.014	3.52
	Half space				

Table 8: Inversion results for bottom model M4 with layer thicknesses estimated from data

Freq. (Hz)	Layer No.	True values			Starting values		Layer thicknesses from data Results of inversion		
		Layer Thick (m)	Comp. wave Spd (m/s)	Density Gm/cc	Comp. wave Spd (m/s)	Density (gm/cc)	Layer Thick (m)	Comp. wave Spd (m/s)	Density Gm/cc
50 to 110	Layer 1	18	1680	1.6	1600	1.7	17	1687	1.618
	Layer 2	12	1500	1.6	1600	1.7	13	1513	1.618
	Half Sp.		1850	1.6	1880	1.7		1857	1.578
250 to 310	Layer 1	18	1680	1.6	1600	1.7	19	1682	1.619
	Layer 2	12	1500	1.6	1600	1.7	12	1569	1.619
	Half Sp.		1850	1.6	1900	1.7		1850	1.700
900 to 960	Layer 1	18	1700	1.6	1600	1.7	18	1697	1.602
	Layer 2	12	1550	1.6					
	Half Sp.		1850	1.6	1900	1.7		1900	1.700

Table 8A: Deviation (Dev) and resolution lengths (RL) for the inverted model in the range-dependent case (Bottom model M4: Two layer model)

Freq.range	Layer	Wave speed (m/s)		Density (gm/cc)	
		Dev (m/s)	Res. Length (m)	Dev (gm/cc)	Res. Length (m)
50 Hz to 110 Hz	Water col	0.0259	1.38		
	Layer 1	4.34	1.85	0.0075	1.30
	Layer 2	0.96	5.42	0.0075	2..00
	Half space	9.59	14.85	0.0094	8.00

Table 8B: Deviation (Dev) and resolution lengths (RL) for the inverted model in the range-dependent case (Bottom model M4: Two layer model)

Freq.range	Layer	Wave speed (m/s)		Density (gm/cc)	
		Dev (m/s)	Res. Length (m)	Dev (gm/cc)	Res. Length (m)
250 Hz to 310 Hz	Water col	0.33	2.26		
	Layer 1	16.25	1.90	0.012	1.01
	Layer 2	0.35	4.62	0.012	2.34
	Half space	0.20	9.10		

C. Range Dependent Case: Three Layer Bottom Model

Region I has three distinct areas with depths of 72 m, 69 m, and 60 m respectively. The bottom model in the three areas has three layers terminated by a half space. The bottom model for areas with depths 72 m and 69 m are the same namely model M1. Area with a depth of 60 m has a different bottom model (M2). The layering of sediment is identical in all the three areas. The layer thicknesses of the three layers are 8 m, 16 m, and 8 m. This is followed a terminating half space. For the bottom model M1, the compressional wave speed of the sediment in the three layers are 1569 m/s, 1705 m/s, and 1530 m/s respectively. In the case of bottom model M2 the compressional wave speed in the sediment layers are 1530 m/s, 1660m/s, and 1490 m/s. The compressional wave speed in the terminating half space is 1850 m/s for all the areas. The density of the sediment is 1.6 gm/cc in the sediment layers and in the half space. In performing the analysis, mode travel time estimates were determined from the signals acquired by Buoys 2, 19, and 20. The ranges and the corresponding depths are listed in Table 1. Prior to performing inversions, the layering of the sediments was estimated using the procedure outlined in Section 3.2. The results of layering structure are detailed in Table 9. The modes that were used in the inversions are indicated in Table 10.

Table 9: Layer thickness estimated from data

Freq. Range (Hz)	Total Thickness (m)	No. of Layers	Layer 1 (m)	Layer 2 (m)	Layer 3 (m)
50 – 110	34	3	10	13	11
250 - 310	35	3	6	19	10

Table 10: Details of modes used in inversion

Frequency range	Mode numbers	Comment
50 Hz – 110 Hz	Modes 1-4	For Buoys 19 and 20: 50 Hz – Modes 1 - 2 60 Hz – Modes 1- 3 70 Hz - Modes 1– 3 80 Hz - Modes 1 - 4 90 Hz - Modes 1 - 4 100 Hz - Modes 1 - 4 110 Hz – Modes 1 - 4 For Buoy 2: 50 Hz - Modes 1 - 2 60 Hz - Modes 1 - 2 70 Hz – 90 Hz – Modes 1 - 3 100 Hz -110 Hz - Modes 1 - 4
250 Hz – 310 Hz	Buoys 19 and 20: Modes: 2 to 10 Buoy 2: Modes 1 to 9	Buoy 19 and 20: Modes 2 to 10 Buoy 2: Modes 1 to 8 at 250 Hz and 260 Hz. Modes 1 to 9 at other frequencies.

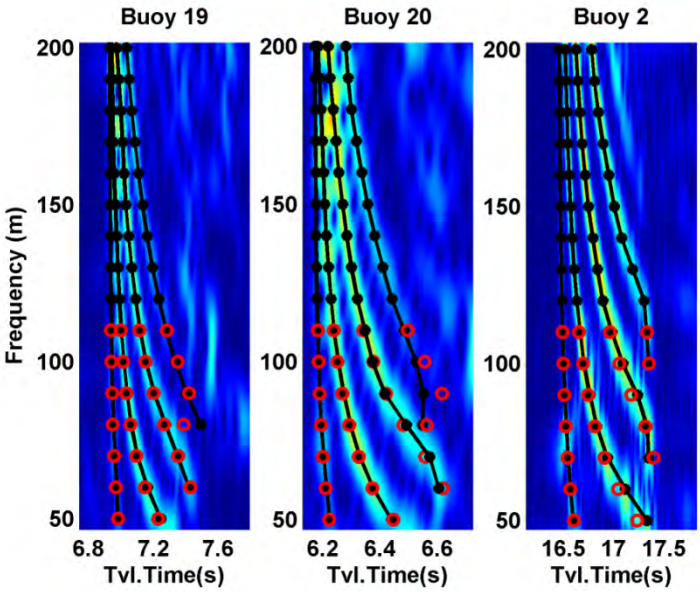

Figure 11: Mode travel time estimated from signals acquired at the three buoys are overlaid over the spectrogram. These are shown in black dots and black lines connecting them. Also shown are the mode travel values predicted by the inverted bottom model at the frequencies (50 Hz – 110 Hz) used in the inversion. These are indicated in red circles.

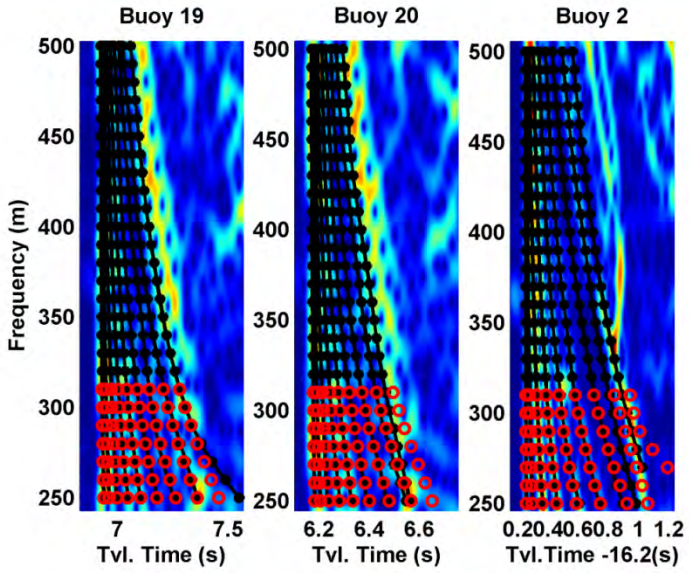

Figure 12: Mode travel time estimated from signals acquired at the three buoys are overlaid over the spectrogram. These are shown in black dots and black lines connecting them. Also shown are the mode travel values predicted by the inverted bottom model at the frequencies (250 Hz – 310 Hz) used in the inversion. These are indicated in red circles.

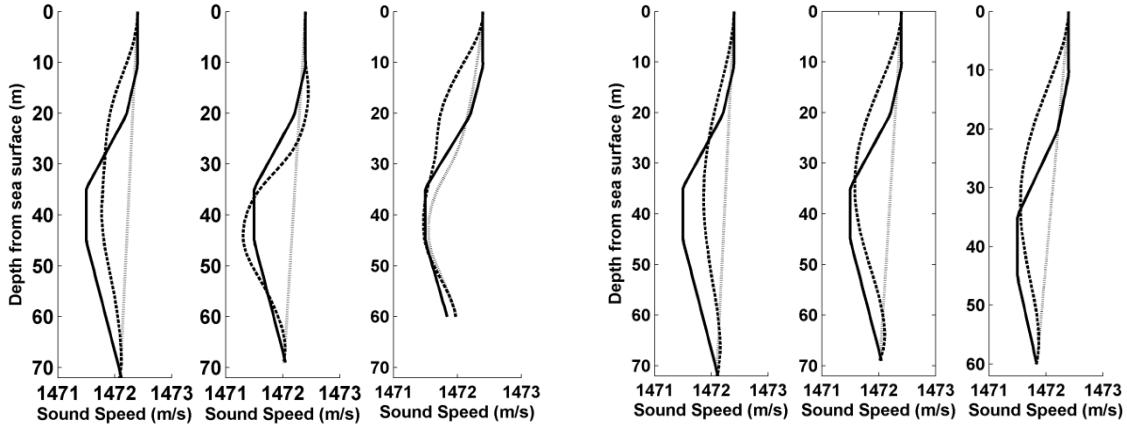

Figure 13: The water column sound speed profiles estimated using mode travel time data are shown above. In each set the three profiles refer to the inversion results for areas with depths of 72 m, 69 m, and 60 m respectively. The left panel shows the results from data in the frequency interval 50 Hz – 110 Hz. The right panel shows the result of inversions using data in the frequency range 250 Hz to310 Hz. In all these plots, the dotted black line is the starting profile, the black line is the true profile and the dashed black line is the inverted profile.

Table 11: Inversion results for Region I (Bottom Model M1) with layer thicknesses estimated from data

Freq. (Hz)	Layer No.	True values			Starting values		Layer thicknesses from data Results of inversion		
		Layer Thick (m)	Comp. wave Spd (m/s)	Density Gm/cc	Comp. wave Spd (m/s)	Density (gm/cc)	Layer Thick (m)	Comp. wave Spd (m/s)	Density Gm/cc
50 to 110	Layer 1	8	1569	1.6	1600	1.7	10	1576	1.571
	Layer 2	16	1705	1.6	1600	1.7	13	1704	1.571
	Layer 3	8	1530	1.6	1600	1.7	11	1574	1.571
	Half Sp.		1850	1.6	1880	1.7		1837	1.598
250 to 310	Layer 1	8	1569	1.6	1600	1.7	6	1582	1.598
	Layer 2	16	1705	1.6	1600	1.7	19	1694	1.598
	Layer 3	8	1530	1.6	1600	1.7	10	1588	1.598
	Half Sp.		1850	1.6	1900	1.7		1837	1.700

Table 11A: Deviation (Dev) and resolution lengths (RL) for the inverted model in the range-dependent case (Area with depth = 72 m)

Freq. Range	Layer	Wave speed (m/s)		Density (gm/cc)	
		Dev (m/s)	Res. Length (m)	Dev (gm/cc)	Res. Length (m)
50 Hz to 110 Hz	Water col	0.05	2.89		
	Layer 1	9.05	1.39	0.014	1.49
	Layer 2	8.75	3.19	0.015	3.16
	Layer 3	4.76	4.43	0.015	3.95
	Half space	6.33	4.92	0.033	6.75

Table 11B: Deviation (Dev) and resolution lengths (RL) for the inverted model in the range-dependent case (Area with depth = 72 m)

Freq. Range	Layer	Wave speed (m/s)		Density (gm/cc)	
		Dev (m/s)	Res. Length (m)	Dev (gm/cc)	Res. Length (m)
250 Hz to 310 Hz	Water col	0.011	2.43		
	Layer 1	12.21	1.0	0.015	1.00
	Layer 2	0.90	1.0	0.015	1.00
	Layer 3	0.27	1.84	0.015	2.64
	Half space				

Table 11C: Deviation (Dev) and resolution lengths (RL) for the inverted model in the range-dependent case (Area with depth =69 m)

Freq. Range	Layer	Wave speed (m/s)		Density (gm/cc)	
		Dev (m/s)	Res. Length (m)	Dev (gm/cc)	Res. Length (m)
50 Hz to 110 Hz	Water col	0.06	2.65		
	Layer 1	5.66	1.32	0.013	1.59
	Layer 2	5.76	3.37	0.013	3.35
	Layer 3	3.05	3.94	0.013	3.82
	Half space	4.02	4.66	0.0025	6.16

Table 11D: Deviation (Dev) and resolution lengths (RL) for the inverted model in the range-dependent case (Area with depth = 69 m)

Freq. Range	Layer	Wave speed (m/s)		Density (gm/cc)	
		Dev (m/s)	Res. Length (m)	Dev (gm/cc)	Res. Length (m)
250 Hz to 310 Hz	Water col	0.02	2.35		
	Layer 1	17.58	1.00	0.015	1.001
	Layer 2	2.12	1.003	0.015	1.002
	Layer 3	0.64	2.38	0.015	2.60
	Half space				

Table 12: Inversion results for Region I (Bottom Model M2) with layer thicknesses estimated from data

Freq. (Hz)	Layer No.	True values			Starting values		Layer thicknesses from data. Results of inversion		
		Layer Thick (m)	Comp. wave Spd (m/s)	Density Gm/cc	Comp. wave Spd (m/s)	Density (gm/cc)	Layer Thick (m)	Comp. wave Spd (m/s)	Density Gm/cc
50 to 110	Layer 1	8	1530	1.6	1600	1.7	10	1526	1.613
	Layer 2	16	1660	1.6	1600	1.7	13	1659	1.613
	Layer 3	8	1490	1.6	1600	1.7	11	1561	1.613
	Half Sp.		1850	1.6	1880	1.7		1838	1.639
250 to 310	Layer 1	8	1530	1.6	1680	1.7	6	1531	1.604
	Layer 2	16	1660	1.6	1680	1.7	19	1658	1.604
	Layer 3	8	1490	1.6	1680	1.7	10	1658	1.604

Freq. (Hz)	Layer No.	True values			Starting values		Layer thicknesses from data. Results of inversion		
		Layer Thick (m)	Comp. wave Spd (m/s)	Density Gm/cc	Comp. wave Spd (m/s)	Density (gm/cc)	Layer Thick (m)	Comp. wave Spd (m/s)	Density Gm/cc
	Half Sp.		1850	1.6	1880	1.7		1849	1.700

Table 12A: Deviation (Dev) and resolution lengths (RL) for the inverted model in the range-dependent case (Area with depth = 60 m)

Freq. Range	Layer	Wave speed (m/s)		Density (gm/cc)	
		Dev (m/s)	Res. Length (m)	Dev (gm/cc)	Res. Length (m)
50 Hz to 110 Hz	Water col	0.007	2.96		
	Layer 1	12.25	1.02	0.01	1.11
	Layer 2	5.89	2.65	0.01	2..33
	Layer 3	6.33	3.79	0.01	3.98
	Half space	10.47	3.67	0.011	6.09

Table 12B: Deviation (Dev) and resolution lengths (RL) for the inverted model in the range-dependent case (Area with depth = 60 m)

Freq.range	Layer	Wave speed (m/s)		Density (gm/cc)	
		Dev (m/s)	Res. Length (m)	Dev (gm/cc)	Res. Length (m)
250 Hz to 310 Hz	Water col	0.01	2.00		
	Layer 1	5.91	1.00	0.013	1.00
	Layer 2	17.07	1.00	0.013	1.00
	Layer 3	18.64	1.27	0.013	1.25
	Half space	23.45	4.38	0.0065	4.54

The Figures 11 and 12 shows the agreement between the mode dispersion data estimated from the signals received at Buoys 19, 20, and 2 and the mode dispersion data predicted by the inverted bottom model. As seen from Figure 11 the agreement in respect of the values in the frequency band 50 Hz to110 Hz is good in most of the points. Even at those points where there is a difference, the differences are quite small. Figure 12 shows the agreement between the experimental estimates and the values predicted by the bottom model in respect of analysis in the frequency band 250 Hz -310 Hz. The modes displayed in the figure are for Modes 2 to 10 for Buoys 19 and 20. The agreement in respect of Modes 2 to 8 is quite good. In respect of the other two modes, there is a wide disparity between the experimentally determined values and the values predicted by the bottom model. These higher order modes are the ones that are corrected during the inversion process due to presence of resonance and corrections carried out as indicated in the Appendix. This has resulted in larger errors between the mode dispersion data as obtained from data and the mode dispersion estimated from the inverted bottom model. In the case of Buoy 2, the modes displayed in Figure 12 are for Modes 1 to 9. A large difference is observed between the mode dispersion values obtained from experimental data and the mode dispersion data from bottom model in respect of Modes 8 and 9. Again, these are the higher order modes that are corrected during the inversion process as per procedure in

Appendix. This has resulted in the observed large error. The differences in the layer thickness from its true values are also another reason for the errors.

The water column sound speed profiles obtained by inversion are shown in Figure 13. The left panel in the figure shows the initial starting profile, the true profile and the inverted profiles for areas with depths 72 m, 69 m, and 60 m respectively. These were obtained using data in the frequency band 50 Hz to 110 Hz. In the case of inversions done for the water column sound speed profile for areas with depth of 60 m, we adopted a mean profile based on the results from areas with depths 72 m and 69 m as the initial profile. The inverted profiles for all areas are fairly close to the true value for the regions. The water column sound speed profiles from data at the higher frequency band (250 Hz to 310 Hz) all have similar profiles with trend in its values decreasing from its value at the sea surface to the lowest value at approximately 35 m from the sea surface and then increasing to the initial value at the sea floor. In obtaining inversion, results for area with depth of 60 m the inverted water column sound speed results for areas with depths 72 m and 69 m were used as input and errors in these input data will affect the results obtained.

The estimates of the compressional wave speed in the top two layers are consistent with the true bottom model. The values for the third layer have large errors both in the frequency band 50 Hz -110 Hz and 250 Hz -310 Hz. The likely cause of this error in respect of inversions in the frequency band 50 Hz -110 Hz are the differences in layer thicknesses from its true value and the errors in the estimated mode dispersion data. In respect of inversions in the frequency band 250 Hz to 310 Hz the mode function has near zero values at depths greater than 25 m from the sea bottom and hence cannot determine the compressional wave speed in the third layer. The density in the sediment layers is consistent with the true values.

The deviation of the water column sound speed, the compressional wave speed of the sediment layers and the density of the sediment layers are in Tables 11A, 11B, 11C, 11D, 12A, and 12B. The tables also list the resolution length of the inverted results. These values were obtained using the procedure outlined in Section 3.1.

3.4 DETAILS OF BROADBAND COMPONENT OF MOMAX V EXPERIMENT AND DATA ANALYSIS

A. Description of Experiment

The experiment described in this section was part of MOMAX V experiment conducted during March 2011. The complete details of MOMAX V are described in Frisk et al[17], which analyzed the narrowband data collected during the experiment. The experiment included a broadband component in which the ship transmitted broadband signals from several discrete locations. At these locations, the ship was nearly stationary. Three freely drifting MOMAX buoys, named Curly, Larry, and Moe, were deployed before the start of the broadband experiment. The locations of the ship and the buoys are shown in Figure 14. The ship had a J15 source suspended at a nominal depth of 56 m. The signal transmitted was an LFM sweep from 50 Hz to 300 Hz. The duration of each ping was 0.5 sec. The pings were repeated every 3 sec for a total duration of 3.5 minutes from each ship location. The MOMAX buoys had two hydrophones at nominal depths of 61 m and 64 m. It is, however, mentioned that source and receiver depths are not required for the estimation of mode arrival times though the location of the source and receiver will determine the modes that are excited.. Data from 21 consecutive transmissions from each of the waypoints are summed up in order to improve the signal to noise ratio. Time synchronization was achieved by recording the transmitted signal on a hydrophone attached to the source frame. There were 14 waypoints at which the ship was nearly stationary and broadband signals were transmitted. The signals received by Curly at one of the hydrophones

were used in the analysis. The signals received from transmissions at waypoints 1 to 10 were used in the analysis. Transmissions from waypoints 11 to14 have low SNR due to large distances between source and receiver and hence were not included in the analysis.

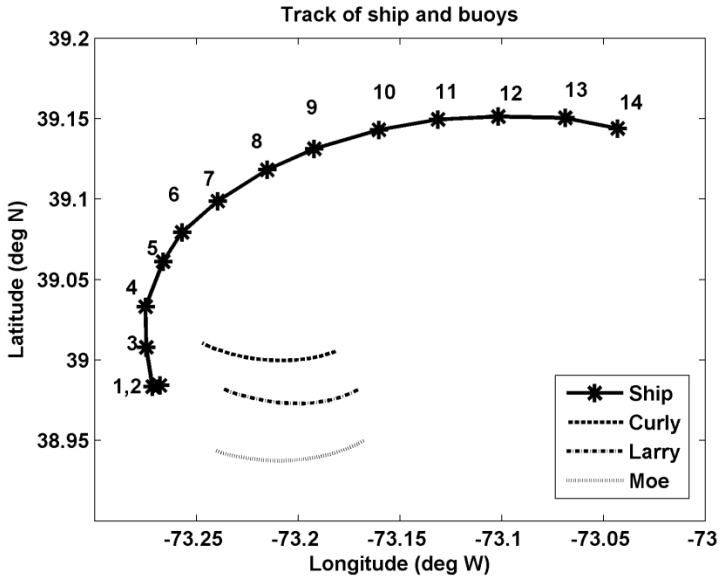

Figure 14: The tracks of ship and buoys during the broadband experiment. The star represents waypoints (numbered 1 to 14) at which the ship was nearly stationary.

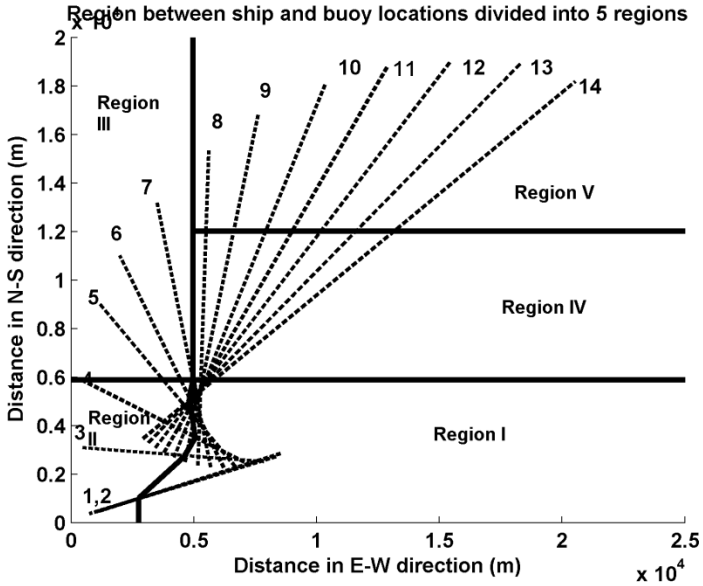

Figure 15: The five regions into which the area is divided and for which the water column sound speed profiles and sediment compressional wave speed profiles are estimated. Dashed lines indicate source-receiver paths together with waypoint numbers.

The distances between the ship and the buoys were obtained using the data from GPS units mounted on the ship and the buoys. The bathymetry between the ship and the buoys was obtained from archival data available for the region. Based on differences in bathymetry, the region between the ship and buoy locations

is divided into five regions, as shown in Figure 15. The depths of the water column in Regions I, II, III, IV, and V have an average value of 75 m, 71 m, 69 m, 69 m, and 69 m, respectively. Data used in the inversion are the mode travel times at frequencies 50 Hz to 110 Hz in 10 Hz steps.

Measurements of ocean temperature were made using expendable bathythermograph probes (XBT) during the course of the experiment. The temperature profiles from XBT measurements together with the values of salinity obtained CTD measurements made during the narrowband experiment. provided the information necessary to obtain the initial sound speed profile for the water column at each location of the XBT.

B. Analysis of Data

In a previously published paper[18], the broadband data collected during the MOMAX V experiment were used to determine the variability in the sound speed profile of the water column with respect to space and time. The sediment compressional wave speed properties from previous inversions done with narrow band data were used as known input data in performing the analysis. A more detailed knowledge was not necessary as only the lower order modes from higher frequencies with limited bottom penetration were used in the analysis. In contrast, we present results of the analysis of the broadband data to estimate simultaneously the three dimensional water column and sediment compressional wave speed and density profiles for the entire region.

The sea bed in the New Jersey shelf has been studied by a number of investigators [19, 20]. A large area of the shelf was also surveyed by CHIRP sonar and other means during the Shallow Water Experiment 2006[21]. A dominant feature of sediment structure as revealed by the survey is the "R" reflector. The reflector is covered by different layers of sediment. These are termed the diffuse outer layer and the inner layered unit. In some areas, another layer termed erose boundary is sandwiched between the layered units. In analyzing data collected during the Shallow Water Experiment 2006 this bottom sediment structure was used to interpret the results. Unfortunately, the area covered by MOMAX V experiment does not fall within the area covered by the surveys. Extrapolating the data from the survey indicates that the inner layered unit is just beneath the ocean bottom and the outer layer and erase boundary are not present[22]. The layering structure of the sediments were estimated using the scheme detailed in Section 3.2. The layering as determined from the analysis of the experimental data indicate the depth of the top layer as 6 m in all the regions. The analysis also revealed a three layer structure for the sediment layers. The layering of the sediment in the different regions as estimated from data are 6 m, 14 m, and 9 m for Regions I and II, 6 m, 14 m, and 10 m for Region III and 6 m, 16m, and 10m for Regions IV and V.

The initial sound speed profiles used to invert for the water column sound speed profiles were computed using the temperature vs depth values obtained from the XBT data collected at locations close to waypoints 1, 4, 6, and 8 and with the salinity value of 33.25 ppt. This value of salinity is based on the spread of salinity values recorded by CTDs deployed in the same general area during the narrowband component of the experiment. While inverting for the sound speed values in Regions II and I, a mean profile based on XBT values at waypoints 1 and 4 was used (cf. Figure 15). In the case of Region III, the initial profile was based on the XBT data from waypoint 6 and a salinity value of 33.25 ppt. In the case of Regions IV and V, the initial sound speed profile used for inversion was based on XBT data from waypoint 8 and a salinity value of 33.25 ppt. The initial profiles and in the inverted profiles are shown in Figure 16.

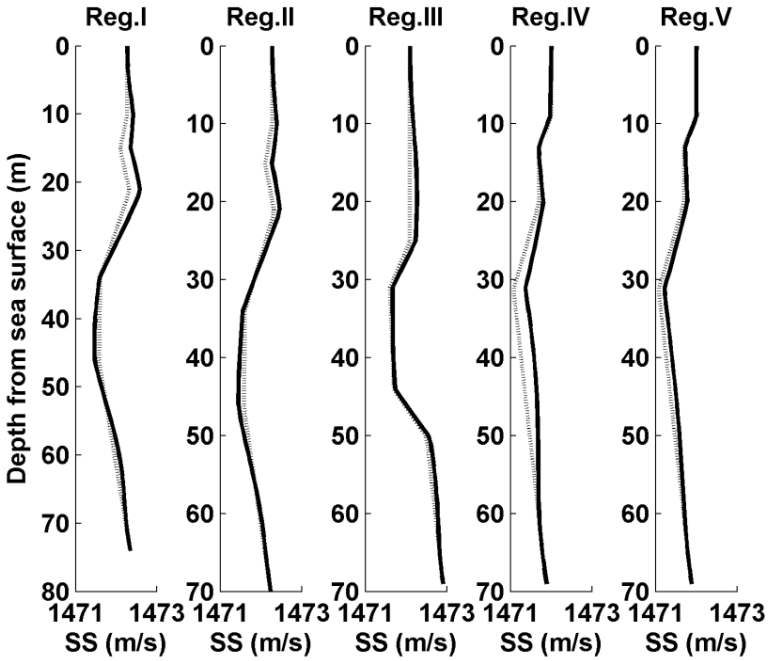

Figure 16: The inverted water column sound speed profiles (solid lines) for the five regions along with the initial background profiles (dotted lines).

The sediment compressional wave speeds and density for the layers as determined by the inversion are listed in Tables 13 and 14. The values for the three layers are close to one another for Regions I, II, and III. In the case of Region V, we see that the compressional wave speed values in the top layer (Layer 1 in Table 13) are much lower than the values for the top layer in the other four regions. This behavior indicates that the sediment properties along the paths between source and receiver for waypoints 8, 9, and 10 are different from the sediment properties along the paths from waypoints 1 to 7.

In the case of the inversions for the sound speed profiles in the water column, the mean deviations in the estimates of the sound speed (m/s) were 0.05, 0.03, 0.02, 0.035, and 0.02 for the five regions, respectively. The mean resolution lengths (m) of the water column sound speed for the five regions are 2.36, 2.29, 1.66, 2.59, and 2.66 respectively. The deviation of the compressional wave speed and the density in inversion results of all the five regions are in Tables 15 and 16. In order to obtain the data covariance matrix, individual pings from the source to the receiver were analysed and the mode travel time for the modes at the various frequencies were estimated. The model covariance matrix were the estimated using Eq.(17. The diagonal of the model covariance matrix provides an estimate of the variance of the model parameters. The deviation for the Layer 3 (i.e. at depth greater than 22 m from ocean bottom) is much smaller than at other depths in respect of Regions IV and V. This is mainly because the mode function values at these locations is very small and therefore estimates of the deviations at these locations tend to be low and hence are not representative of the deviation in the sediment layers. In obtaining deviation of the inverted parameters no prior variance has been assumed and therefore does constrain the solution. The tables also include values of resolution lengths in all the cases.

3.5. DISCUSSION OF RESULTS OF EXPERIMENTAL DATA ANALYSIS

A. Comparison of Experimentally Measured Mode Dispersion with Model Predictions

Figure 17 shows the spectrogram of the signals at waypoints 1, 6, and 8 with the mode dispersion as predicted by the models obtained by the inverse. The figures show good agreement between the data and model predictions based on the inverted model.

B. Comparison with Other Geoacoustic Models Determined during the Narrowband Experiment

The broadband experiment considered here was one component of MOMAX V. The other part consisted of a narrowband experiment in which CW tones at a set of frequencies were broadcast from a moving source. Two freely drifting buoys (Shemp and Larry) were deployed during this part of the experiment. The details of the experiment are explained in Ref. 17, and the tracks of the ship and the buoys are shown in Figure 18. As seen in this figure, the narrowband experiment was conducted in the general area covered by transmissions from waypoints 3 and 4. The ship's track during the narrowband experiment for the most part lies in Region II and is bounded by the source/receiver paths from waypoints 3 and 4.

The bottom models obtained from the narrowband data and the broadband data are compared in Table 17. The values of the compressional wave speeds in the top two layers of Region II are consistent with the values obtained in the narrowband experiment based on the data collected by Shemp and Larry. With respect to the third layer, the values from broadband data are consistent with the model obtained using data collected by Larry in the narrowband experiment but are significantly different from the values obtained using Shemp data. To understand this discrepancy, we look at the differences in the data collected by Shemp and Larry during the narrowband experiment. The paths between the source and receiver in the case of the narrowband and broadband experiments are shown in Figure 18. The ship's path during transmissions to Shemp and Larry are the same. The location of the buoys are however different with Larry located to the south of Shemp. It is likely that the differences in bottom models obtained from data collected by these two buoys are the result of the areas covered by the transmissions to these buoys. This suggests that the region to the south of the areas covered by transmissions to Shemp have a slightly different bottom especially with respect to the third layer. During the broadband experiment, the data used for inversions in respect of Regions I and II are from transmissions from waypoints 1, 3, and 4. While the paths from waypoints 1 and 3 cover areas to the south of the paths during the narrowband experiment, the path from waypoint 4 cover area to the north of the region covered in the narrow band experiment. However, the inverted profile for sediment compressional wave speed for Region II is similar to that obtained from narrowband data collected by Larry. This suggests that the inverted bottom model for Region II is representative of the sediment in areas south of the paths covered during the narrowband experiment.

Table 13: Compressional wave speed estimates (m/s)

Region	Layer 1	Layer 2	Layer 3	Half space
Region I	1549	1644	1604	1856
Region II	1594	1661	1609	1863

Region	Layer 1	Layer 2	Layer 3	Half space
Region III	1579	1687	1624	1887
Region IV	1533	1638	1592	1870
Region V	1506	1623	1593	1872

Table 14: Density estimates (gm/cc)

Region	Layer 1	Layer 2	Layer 3	Half space
Region I	1.602	1.727	1.612	1.631
Region II	1.520	1.638	1.600	1.620
Region III	1.681	1.694	1.604	1.593
Region IV	1.661	1.680	1.512	1.602
Region V	1.700	1.591	1.540	1.632

Table 15: Compressional wave speed deviations Dev and resolution lengths RL in the sediment for the five regions

Layer	Region I		Region II		Region III		Region IV		Region V	
	Dev. (m/s)	RL (m)	Dev (m/s)	RL (m)	Dev (m/s)	RL (m)	Dev (m/s)	RL (m)	Dev (m/s)	RL (m)
1	10.98	1.0	10.58	1.00	32.28	2.072	8.156	1.0	4.921	1.0
2	4.72	1.001	5.74	1.001	18.62	5.314	12.557	1.001	14.90	1.006
3	5.55	1.028	4.93	1.03	2.71	8.121	1.453	2.36	1.82	2.05

Table 16: Density deviations (Dev) and resolution lengths (RL) in the sediment for the five regions

Layer	Region I		Region II		Region III		Region IV		Region V	
	Dev. (gm/cc)	RL (m)	Dev (gm/cc)	RL (m)	Dev (gm/cc)	RL (m)	Dev (gm/cc)	RL (m)	Dev (gm/cc)	RL (m)
1	0.047	1.077	0.0424	1.104	0.119	1.042	0.0625	1.681	0.036	4.448
2	0.043	1.557	0.0389	1.488	0.191	2.361	0.0602	2.520	0.030	3.30
3	0.0167	4.925	0.0161	4.742	0.055	8.661	0.036	1.920	0.022	2.24

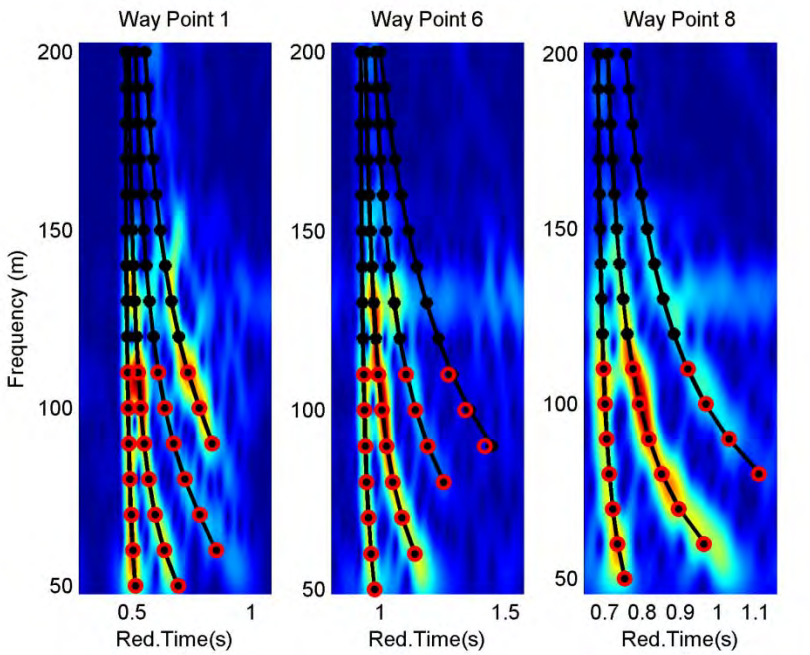

Figure 17: Spectrograms of data received by Curly for transmissions from waypoints 1, 6, and 8. The mode dispersion curves estimated from the data are overlaid. The red circles in the plots indicate the mode travel time as predicted by the inverted bottom model.

Table 17: Inverted bottom models for Region II from narrowband and broadband experiments

Experiment	Layer 1. Wave speed (m/s)	Layer 2 Wave speed (m/s)	Layer 3 Wave speed (m/s)	Half space Wave speed (m/s)
NB/Larry/SB795	1588	1702	1657	1850
NB/Shemp	1568	1705	1527	1850
BB/Region II	1594	1661	1609	1863

We now try to predict the pressure fields measured in the narrowband experiment using the inverted bottom model for Region II from the broadband experiment. In computing the pressure fields, all other parameters from the narrowband experiment such as the water column sound speed profile, the range-dependent bottom depths, and the source and receiver depths were used. The only differences were the geoacoustic parameters of the bottom. The pressure fields were computed at four frequencies, i.e., 50 Hz, 75 Hz, 125 Hz, and 175 Hz, using the normal mode code KRAKEN[13]. These fields are plotted against the fields measured by Shemp and Larry during the experiment and are shown in Figures 20 and 21.

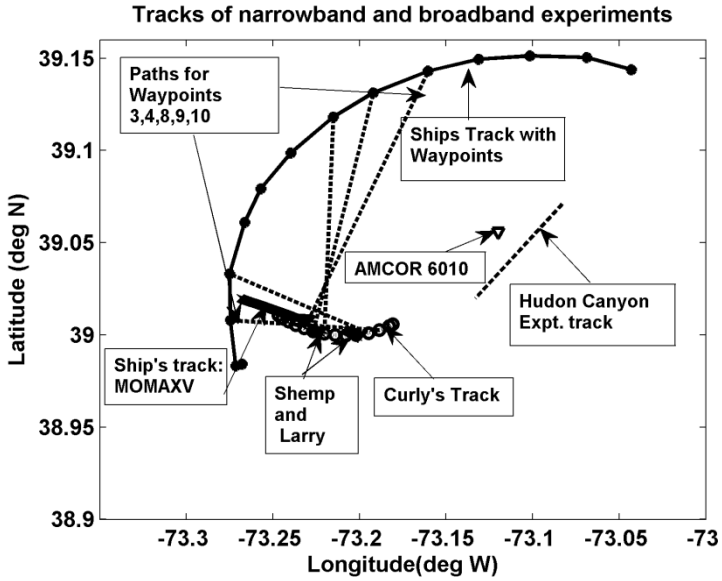

Figure 18: The ship's track and the buoy's (Curly) track during the experiment are shown in the figure. The tracks of the ship and the buoys during the MOMAX V narrowband experiment are also indicated.

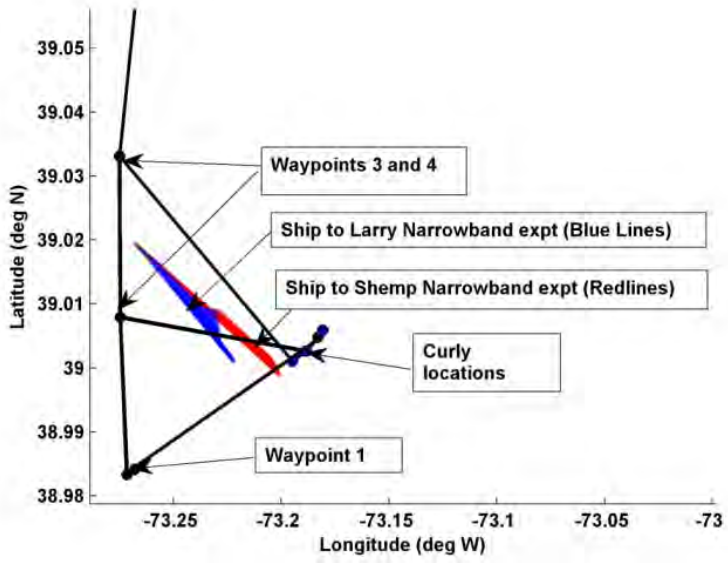

Figure 19: The paths between the source and receiver in the case of the narrowband and broadband experiments.

With respect to the fields measured by Shemp and Larry during the narrowband experiment, we note that the agreement between the measured and predicted fields is better in respect of the field measured by Larry and the predicted field. It is also seen that the bottom models based on Larry data has a better agreement with the inverted profile from the broadband data as seen in Table 17. To further assess agreement between the two results, we look at the corresponding wavenumber spectra. In Figures 22 and 23 the wavenumber spectra obtained from the fields predicted by the broadband model are plotted against the wavenumber spectra obtained from the fields measured during the narrowband experiment. There is good agreement

between the two in the case of strong lower order modes. The differences are pronounced in the case of higher order modes. This indicates that the dominant interference pattern, which is due to the lower order modes, will approximately be the same for both cases. The differences in the wavenumber spectra of the higher order modes will manifest themselves as differences in the pressure fields that are superimposed upon the dominant interference pattern. This behavior is also observed in the plots shown in Figures 20 and 21.

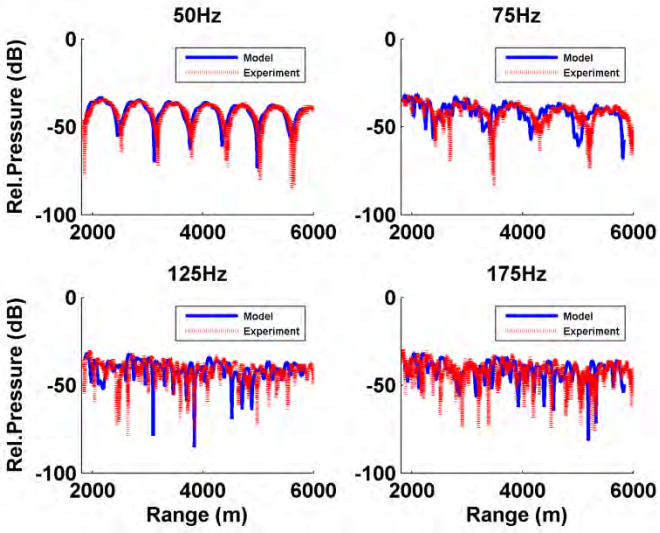

Figure 20: The pressure fields measured by Shemp during the narrowband experiment and the fields predicted by the Region II broadband model.

C. Comparison with Other Bottom Models

The sediment in the New Jersey shelf area can be classified as sandy clay, clay or silty clay. The compressional wave speed values, density values and their standard deviations for these types of sediments in the continental shelf areas are tabulated in Table 18 [23].

Table 18: Sediment type and their typical properties from Reference 23

Type of sediment	Comp. wave speed (m/s)	Standard deviation	Density(gm/cc)	Standard deviation
Sand-silt- clay	1579	8	1.596	0.022
Silt	1615	8	1.740	0.047
Silty clay	1520	3	1.421	0.013

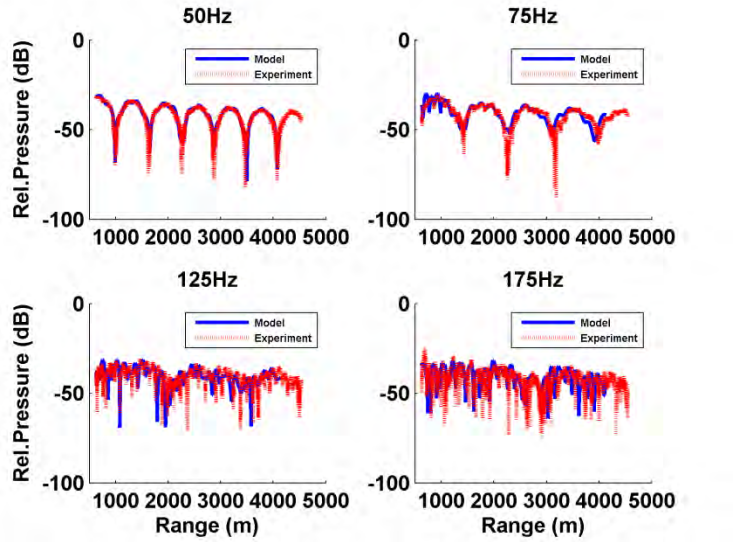

Figure 21: The pressure fields measured by Larry during the narrowband experiment compared with the fields predicted by the bottom model obtained from the broadband experiment.

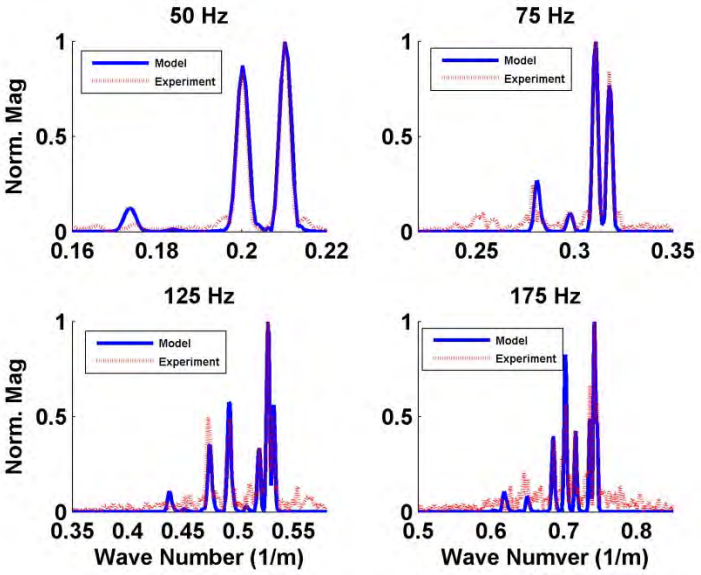

Figure 22: The wavenumber spectra obtained from the measured fields compared with the wavenumber spectra obtained from the predicted fields for the Shemp model.

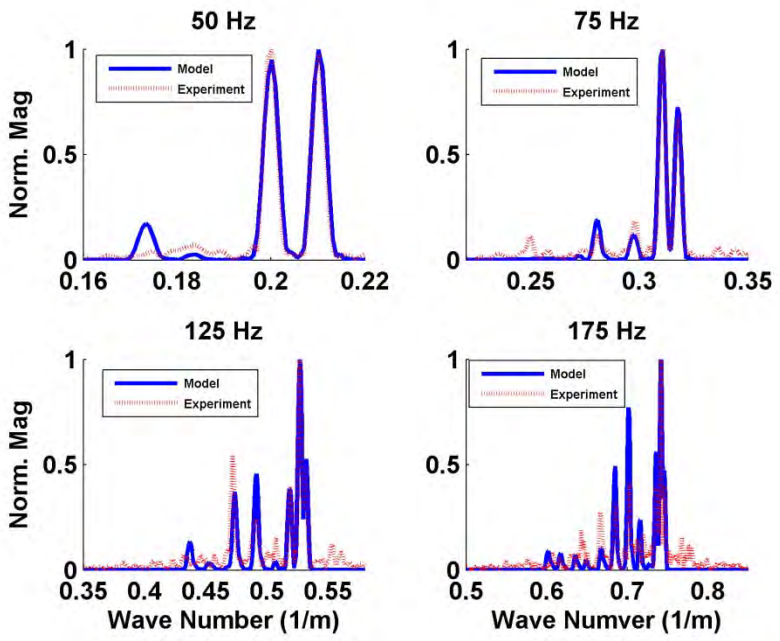

Figure 23: The wavenumber spectra obtained from the measured fields compared with the wavenumber spectra obtained from the predicted fields for the Larry model.

The New Jersey shelf area has been the site of several acoustic experiments. The compressional wave speed results of the four experiments that took place in the general area of the SW06 experiment are summarized in Ref. 17 and reproduced here in Table 19. The layered unit, the layer below 'R' reflector, and the deep low speed layer in Table 19 correspond to layers 1 to 3 in Table 13, where estimates from analysis of MOMAX V are tabulated. The values of sediment compressional wave speeds for each sediment unit estimated using MOMAX V data are in general agreement with the compressional wave speeds values as indicated in Ref. 23 and the speeds estimated during the SW06 experiment[1,,8,,,24,25,26]. Differences present in the estimated values from different experiments may be attributed to spatial variability within each unit, the parameterization of the inversion technique, as well as the frequency band used in obtaining the results. The bottom models obtained in earlier SW06 experiments do not indicate the presence of a deep low speed layer below the 'R' reflector as is the case with the models from the MOMAX V experiment. However, analysis of data acquired near AMCOR site 6010 during an experiment in 1988 (Hudson Canyon Experiment) [27, 28] produced a bottom model with a low speed layer below the reflector. It is mentioned that the location of the Hudson Canyon Experiment is to the east of the region covered by the MOMAX V experiment.

In the case of experiments conducted during SW06, only two experiments estimated the density values from experimental data. In other cases, the values were assumed based on some archival data or in one case based on porosity data. In the case of the experiments which estimates the density values from the experimental data, there is general agreement between these estimated values and that predicted by MOMAX V.

Table 19: Summary of previous results compressional wave speed (All values in m/s)

Reference	Layered unit	Below 'R' reflector	Deep low speed layer
Ballard et.al[8]	1580+/-19	1725+/-15	
Rajan et.al[1]	1510-1650	1650-1850	
Jiang et.al[24]	1572+/-15	1740+/-40	
Knobles et.al[25,26]	1580-1595	1720	
Cederberg et al[27] Cederberg et al[28]	1510-1550	1770-1790	1670
Region I	1569	1644	1604
Region II	1594	1661	1609
Region III	1579	1687	1624
Region IV	1533	1638	1592
Region V	1506	1623	1593

4.0 RESULTS AND PROJECT'S ACCOMPLISHMENTS

In this paper, we present results of simulation study and analysis of field experimental data to evaluate the ability of inversion methodology to estimate the acoustic properties over a wide area of a shallow water region using a distributed net work of receiver sonobuoys and a single source sonobuoy. The bathymetry in shallow water areas are complex giving rise to varying water column depths as well as varying sediment characteristics. In order to represent such an environment in the simulation, an area off the coast of New Jersey for which the bathymetry is well known was used in this simulation. This selected area was subdivided in to six regions each with their own areas of varying depths. Dependng on the varying depths of water column we assumed different sediment propertes. A number of receiver sonobuoys were distributed over the entire area and a source sonobuoy was placed in the middle of the distributed net work of receiver sonobuoys. The source transmitted a broadband signal and these signals were acquired by the receiver sonobuoys. Based on the bathymetry, the tracks between the source and receiver the problem is either range independent or range dependent. The water column sound speed was assumed to be the same over the entire region. The signals at the receiver buoys were computed numerically and this was analysed to estimate the mode dispersion data. This was carried out with the source signal at different frequency bands. The mode dispersion data thus obtained were used to estimate the water column soud speed profile,

the compressional wave speed profile of the sediment layers and the density profiles of the sediment. Similar estimates were obtained for the half space parameters as well. The analysis also included estimates of the total layer tickness, the number of layers, and the thicknesses of each layer. In the analysis presented in the paper the results for the range independent case shows that the estimates of water column and sediments properties are close to the true value in the frequency band 50 Hz to 110 Hz. At higher frequency band (250 Hz to 310 Hz) the sediment properties have larger difference from its true values at depths where the mode function has close to zero amplitude. The agreement between the mode dispersion data from the acquired signal and that obtained from the bottom model are in excellent agreement. In the case of range-dependent case with a two layer bottom model the inversion results for the water column sound speed profile is consistent with the true model in all the three frequency bands. The sediment properties estimated in the frequency band 50 Hz to 110 Hz are close to the true bottom model. In the higher frequency bands inversions were able to determine the parameters of the top layer only because of the mode functions having near zero values at the depths of the second layer. Similar results were obtained in the case of range-dependent case covering three layer bottom model. The best results were obtained in the frequency band 50 Hz to 110 Hz. In the higher frequency band inversion results were consistent with the true values for the top layer. These results demostrate that inversions based on mode dispersion data using linearized inversion procedure can yield meaningful results of the water column and sediment properties. The scope of the inversion results deteriorates with the increase in the frequency band of the signal.

The broadband data obtained during the MOMAX V experiment were processed to invert simultaneously for the 3D compressional wave speed and density profiles of the seabed and sound speed profiles in the water column. The experimental data were acquired on a set of freely drifting, GPS-navigated buoys and a nearly stationary, low-frequency (50-300 Hz) sound source at a set of fixed locations. Bottom models for sediment properties over a wide geographical area were estimated and validated by comparing them with the bottom models obtained from the narrowband data acquired during the same experiment. Further validation was done by comparing the pressure fields computed using the broadband bottom models with the fields measured during the narrowband experiment. Also, the bottom models from the broadband experiment were compared with models obtained from other experiments, and it was shown that the models are consistent with one another.

Overall, these results show that data collected by a distributed network of buoys can be used to obtain the water column sound speed profiles,sediment compressional wave speed profiles and sediment density profiles over a wide area.

Table 20: Summary of previous results for density (All values in gm/cc) (Values with * mark were assumed values and not estimated from data, values with # mark were calculated from porosity values measured during AMCOR 6010)

Reference	Layered unit	Below 'R' reflector	Deep low speed layer
Ballard et.al[10]	1.9*	1.9*	
Rajan et.al[2]	1.6*	1.6*	
Jiang et.al[23]	1.68	1.68	
Knobles et.al[24,25]	1.83	1.93	
Cederberg et al[26] Cederberg et al[27]	1.9#	2.1#	2.2#
Region I	1.602	1.727	1.612
Region II	1.520	1.638	1.600

Reference	Layered unit	Below 'R' reflector	Deep low speed layer
Region III	1.681	1.694	1.604
Region IV	1.661	1.680	1.512
Region V	1.700	1.591	1.540

5.0 RECOMMENDATIONS FOR FUTURE TECHNOLOGY OR RESEARCH

This report has used linearized inversion methodology for estimating the water column and sediment properties over a wide area. Other inversion methods, which use full non-linear inversion procedures, can also be used for the analysis of the data. There is however a need to perform a field experiment that is similar to MAC and collect the data acquired by the sonobuoys for analysis. It is proposed that this experiment be done in the area off the New Jersey coast where a number of acoustic experiments have been conducted in the past. It will then be possible to compare the results of the analysis from this experiment with the results from previous experiments.

6.0 CONTRACT COSTS

The program financial status as of 30 September 2018:

	End Date			9/30/2018	
Total Contract Amount			**$63,598**	**$63,598**	**$0**
Base: 0001 / 000101 / AA	9/30/2015	0001	$3,782	$3,782	$0
Option 1: 0002 / 000201 / AB	9/30/2016	0002	$19,816	$19,816	$0
Option 2: 0003 / 000301 / AC	9/30/2017	0003	$20,000	$20,000	$0
Option 3: 0004 / 000401 / AD	9/30/2018	0004	$20,000	$20,000	$0
SUBTOTAL:			*$63,598*	*$63,598*	*$0*

7.0 REFERENCES

[1]S. D. Rajan and K. M. Becker, "Inversion for range-dependent sediment compressional-wave-speed profiles from modal dispersion data", IEEE J. Ocean. Eng., 35, 43–58, (2010).

[2]G.Potty, J. Miller, L. Lynch, and K. Smith, "Tomographic imaging of sediment parameters in shallow water", J. Acoust. Soc. Am, 108, 973-986, 2000.

[3]G.Potty, J. Miller, and J. Lynch, "Inversion for the geoacoustic properties at the New England Blight", J. Acoust. Soc. Am., 114(4), 1174-1187, 2003.

[4]J.Bonnel, S.E. Dosso and N.R. Chapman, "Bayesian geoacoustic inversion of single hydrophone light bulb data using warping dispersion analysis", J. Acoust. Soc. Am., 134(1), 120-130, 2013.

[5]S. D. Rajan, G. V. Frisk, K. M. Becker, J. F. Lynch, G. Potty, and J. H. Miller, "Modal inverse techniques for inferring geoacoustic properties in shallow water", in *Important Elements in* : *Geoacoustic Inversion, Signal Processing, and Reverberation in Underwater Acoustics*, pp 165-234, Edited by A. Tolstoy, Research Signpost, Kerala, India, 2008.

[6]S.D.Rajan, "Simultaneous reconstruction of compressional wave speed and density profiles from modal eigenvalues", Journal of Computational Acoustics, 6(1&2), 257-267, 1994.

[7]L. Simcik and P. Lin, "Qualitative regularization: Resolving non-smooth solutions", Tech Report CSE 94-12, University of California, Department of Mathematics, (1994).

[8]M. S. Ballard, K. M. Becker, and J. A. Goff, "Geoacoustic Inversion for the New Jersey shelf: Three dimensional sediment model", IEEE J. Ocean. Eng., 35, 28–42, (2010).

[9]*Solution of ill-posed problems*, A. N. Tikhonov and V. Y. Arsenin, Hallsted, Washington D.C., (1977).

[10]M.S. Ballard and K.M. Becker, "Optimized constraints for the linearized geoacoustic inverse problem", J. Acoust. Soc. Am., 129(2), 612-621, 2011.

[11]*Quantitative Seismology Theory and Methods Vol II*, K. Aki and P.G. Richards, W.H. Freeman & Co., 1980.

[12]*Spread spectrum systems with commercial applications*, R. C. Dixon, John Wiley & Sons, 1994.

[13]M. Porter, "The Kraken Normal Mode program" SACLANT Undersea Research Center, La Spezia, Italy, Tech Report SM245, (1991).

[14]D. M. F. Chapman and D. D. Ellis, "The group velocity of normal modes", Journal of the Acoustical Society of America, 74, 973-979, 1983.

[15]J. Bonnel, B. Nicholas, J. Mars, and S. C. Walker, "Estimation of modal group velocities with a single receiver for geoacoustic inversion in shallow water", J. Acoust. Soc. Am., 128, 719-727, (2010).

[16]J. Bonnel, C. Gervaise, P. Roux, B. Nicolas and J. Mars, "Modal depth function estimation using time-frequency analysis", J. Acoust. Soc. Am., 130, 61-71, 2011.

[17]G.V. Frisk, K.M. Becker, S.D. Rajan, C.J. Sellers, K. von der Heydt, C. M. Smith, and M.S. Ballard, "Modal mapping experiment and geoacoustic inversion using sonobuoys", IEEE J. Ocean. Eng., 40, 607-620, (2015).

[18]M.S. Ballard, G.V. Frisk, and K.M. Becker, "Estimates of temporal and spatial variability of ocean sound speed on the New Jersey Shelf", J. Acoust. Soc. Am., 135, 3316-3326, (2014).

[19]T.A. Davies, J.A. Austin Jr, H.B. Lagoe and J.D. Millimann, "Late quaternary sedimentation off New Jersey shelf: New results using 3-D seismic profiles and cores", Marine Geology, 108, 323-343, 1992.

[20]J.A. Goff, B.A. Kraft, ,L.A. Mayer, S.G. Schock, C.K. Sommerfield, H.C. Olson, S.P. Gulick and S. Nordfjord, "Seabed characterization on the new Jersey middle and outer shelf: Correlatability and spatial variability of seafloor sediment properties" Marine Geology, 209, 147-172,2004

[21]D. J. Tang, J. Moum, J. Lynch, P. Abbot, R. Chapman, P. Dahl, T. Duda, G. Gawarkiewicz, S. Glenn, J. Goff, H. Graber, J. Kemp, A. Maffei, J. Nash, and A. Newhall, "Shallow Water '06 - A Joint Acoustic Propagation /Nonlinear Internal Wave Physics Experiment," Oceanography. 20, 156–167, (2007).

[22]Private communication from Megan Ballard.

[23]E.L.Hamilton,"Geoacousticalmodeling of the sea floor", Journal of the Acoustical Society of America, 68(5), 1313-1340, 1980.

[24]Y. M. Jiang and N. R. Chapman, "Bayesian geoacoustic inversion in a dynamic shallow water environment", J. Acoust. Soc. Am., 123, EL155–EL161, (2008).

[25]D. P. Knobles, J. A. Goff, R. A. Koch, P. S. Wilson, and J. A. Shooter, "Effect of inhomogeneous sub-bottom layering on broadband acoustic propagation," IEEE J. Ocean. Eng., 35, 732–743, (2010).

[26]D. P. Knobles, P. S. Wilson, J. A. Goff, and S. E. Cho, "Seabed acoustics of a sand ridge on the New Jersey continental shelf", J. Acoust. Soc. Am., 124, EL151–EL156, (2008).

[27]R. J. Cederberg, W. L. Siegmann, and W. M. Carey, "Influence of geoacoustic modeling on predictability of low-frequency propagation in range-dependent, shallow-water environments", J. Acoust. Soc. Am., **97**, 2754–2766, (1995).

[28]R.J. Cederberg, W.M. Carey, and W.L. Seigman, "Modal analysis of geoacoustic influences on shallow water propagation", IEEE J. Ocean. Eng., **22**, 237-244, (1997).

8.0 APPENDIX

To describe the problem encountered while processing data from higher frequencies we look at the spectrogram of the signal received at Buoy 8 in Region 5 using STFT. It is shown in the left panel of Figure A1. The dispersion curves of Modes 2 to 14 as obtained using the warping method is shown overlaid over the spectrogram. It is seen that in the case of all modes the mode dispersion curve varies smoothly over the frequency interval 250 Hz to 500 Hz. In the right panel of Figure A1, we plot the spectrogram plot from data as acquired by Buoy 8 and the dispersion data for Modes 11, 12, and 13 overlaid. The dispersion data for these modes were computed theoretically with the known values of the water column and sediment properties. The dispersion data from theory shows major differences with the data obtained using warping method. The theoretical dispersion curve does not vary smoothly over the frequency range considered. There are abrupt changes in the mode travel times. It is also noticed that part of the mode dispersion curve aligns itself with the dispersion curve of a lower mode. For example, the dispersion curve for mode 13 follows the trajectory of mode 13 in the time frequency plot at higher frequencies. At 340 Hz it breaks out and shows much lower travel time. Then at 310 Hz the dispersion returns to slowly varying travel time. But this part of the dispersion curve now aligns itself with the dispersion curve for mode 12. A similar feature is also seen in the case of mode 12. It is to be noted that dispersion data is computed theoretically for the bottom models at each stage of the iteration in the inversion process and these are to be compared with the estimated data obtained from the spectrogram of the received signal. We have already seen that the dispersion data from the spectrograms do not exhibit such abrupt changes in mode travel times. The sharp deviations from mode travel times occur at frequencies where resonance of mode occur. These modes have near zero mode function amplitudes in the water column but have large values in the sediment layers. These are shown in the left panel of Figure A2. These modes are therefore not seen in the signal acquired by the receivers that are located in the water column.

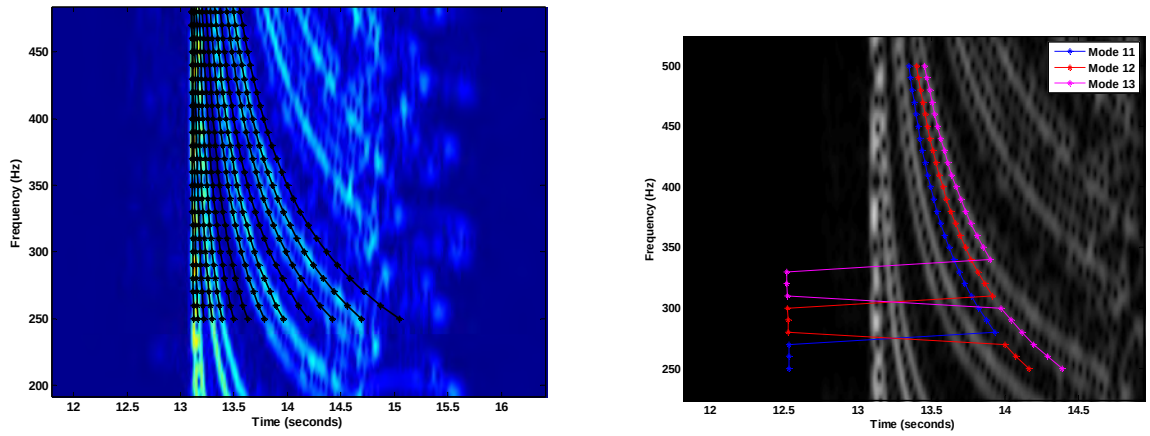

Figure A1: The spectrogram of the data acquired at Buoy 8 located at a range of 19270 m from the source is shown in the left panel. The mode dispersion curves for Modes 2 to 14 obtained using the warping procedure is shown overlaid on the time-frequency plot in the right panel. In the right panel, we have the theoretical mode dispersion curve for Modes 11, 12, and 13 overlaid on the spectrogram.

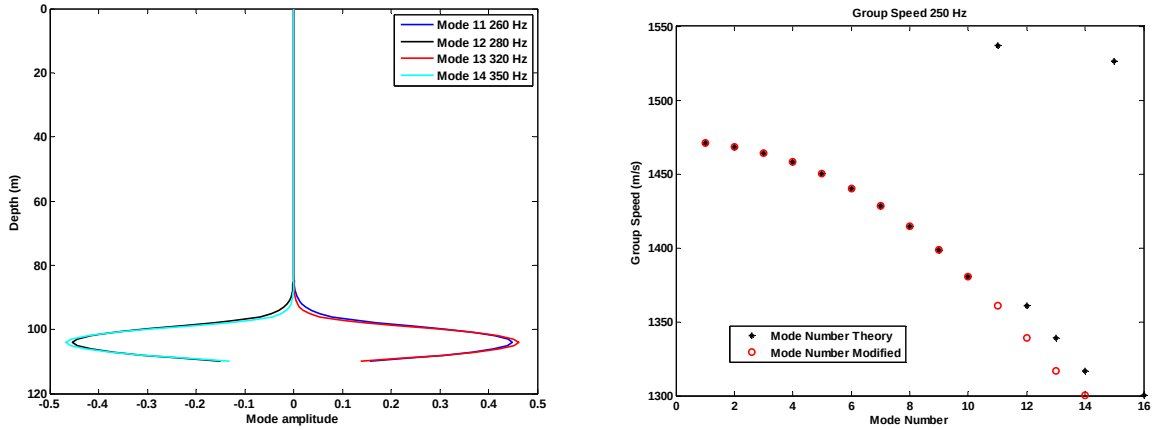

Figure A2: The left panel shows the mode function of the resonant modes. The right panel shows the group speed of Modes 1 – 15 at 250 Hz for bottom model corresponding to M5. The black dots are the theoretical group speed of modes. The red circles are the corrected values of group speed of modes.

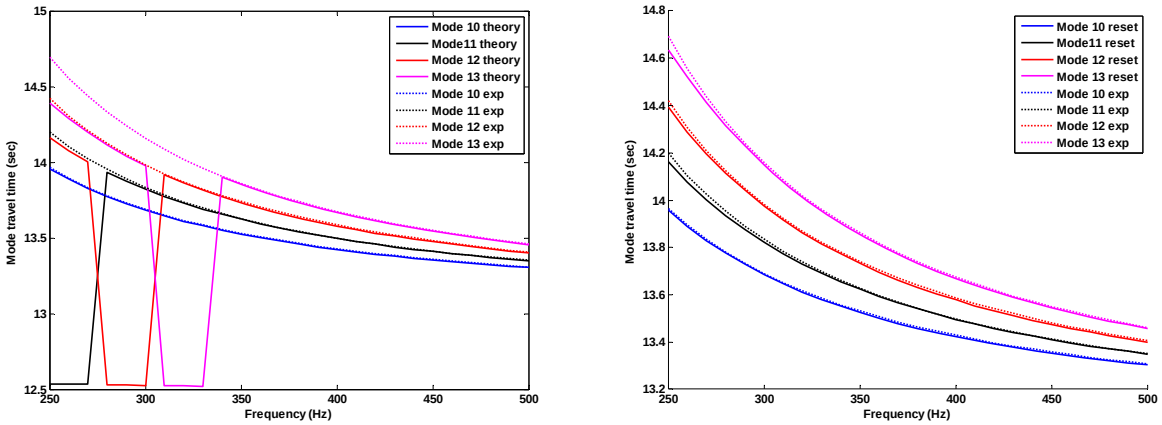

Figure A3: The mode dispersion for Modes 10 to 13 as obtained from theory is compared with the dispersion curve from experiment in the left panel. In the right panel the mode dispersion curve corrected with the procedure that eliminates the outliers is compared with the mode dispersion from experiment. In this case there is good agreement between the two.

Described below is the approach adopted to overcome this problem. In the right panel of Figure A2, we plot the group speed of Modes 1 to 15 at 250 Hz. These are represented by black dots. We notice that two values (i.e. those for Modes 11 and 15) are much higher than the rest. We renumber the modes eliminating the ones that are outliers. We now have 13 modes instead of 15. What was originally mode 12 has now become Mode 11 and so on. This is shown as red circle in the figure. We do this for modes at each frequency and with this; a modified mode dispersion data is obtained. In the left panel of Figure A3, we plot the mode dispersion data as obtained from data for Modes 11, 12, and 13 and compare it with the mode dispersion data as obtained from theory. In the right panel of Figure A3, we plot the theoretical dispersion data as modified by the procedure outlined above. It is seen that the modified dispersion data follow the mode dispersion curves as determined from data. In adopting this procedure, we identified modes for which

sharp increases in the group speed occur and eliminated those modes. Simultaneously we made suitable changes to the mode function of the modes and eigenvalues associated with the modes.

The inversion for the bottom properties were then performed using this corrected information. It is added that since the procedure for inversion is an iterative process starting with an initial bottom model, the presence of outliers in the group speed of modes is checked at each step in the iteration process and corrections made as outlined above. Using this approach inversions for the bottom models were carried out.

DISTRIBUTION LIST

Addressee	**DOD AAD CODE**	**Number of copies**
Dr. Robert Headrick, Code: 32 Office of Naval Research (ONR) 875 North Randolph Street Arlington, VA 22203-1995 REF: N00014-15-P-5114 Email: bob.headrick@navy.mil	N00014	1 (Emailed)
Director, Naval Research Lab Attn: Code 5596 4555 Overlook Avenue, SW Washington, DC 2037-5-5320 Email: reports@library.nrl.navy.mil	N00173	1 (Emailed)
Defense Technical Information Center 8725 John J. Kingman Road STE 0944 Ft. Belvoir, VA 22060-6218 Email: tr@dtic.mil	HJ4701	1 (Emailed)
Administrative Contracting Officer Email notification only to: theresa.g.enkosky.civ@mail.mil	S2206A	1 (Transmittal Letter Only)
Scientific Solutions, Inc. 99 Perimeter Road Nashua, NH 03063-1325	Cage Code: 0VH19	1 (Contract Files)